Universiteit Utrecht

MASTER THESIS

*Degree in Experimental Physics*

---

# Imaging through scattering media

---

**Wavefront shaping and memory effect**


*Author:*
TOMMASO PAVOLINI BSC
*Student number:*
5998700

*Supervisors:*
PROF. DR. ALLARD P. MOSK
DR. IR. SANLI FAEZ
JEROEN BOSCH MSC


13th July 2018

*"Non c'é cena o pranzo o soddisfazione del mondo, che valga una camminata senza fine per le strade povere dove bisogna essere disgraziati e forti, fratelli dei cani."*

Pier Paolo Pasolini

UTRECHT UNIVERSITY

# *Abstract*

Experimental Physics

Graduate School of Natural Sciences

Experimental Physics

**Imaging through scattering media**

by Tommaso PAVOLINI

In this project, Imaging through scattering media, we create an intensity-enhanced focus and scan it around by using the memory effect. Limitations and problems found during the process are described in this thesis. We describe how two techniques could be implemented to check if imaging through wavefront shaped focus works in reflection too.

# *Acknowledgements*

I want to thank all the people in the Nanophotonics group: I have really enjoyed my stay here.

Many thanks to all the students: Tang, Lorenzo, Peter, Vasilis, Alberto, Charly, Sanne and every Bachelor's and Master's student whom I met. And sorry for the loud music!

Many many thanks to Jeroen who led me along the whole period of this project. Also, many thanks to Π, Abhi, Dashka, Sebas, Jasper, Javi and every PhD (and PhD candidate): you were able to tolerate my presence and give me many hints and suggestions.

Many thanks to Dante, Paul, Cees and Mijke for technical and bureaucratic help and for the conversations in the corridors.

Many thanks to Allard who allowed me to work, try, fail and learn on this topic in this group. Many thanks for the sharp observations and lucid reasonings that you always bring to discussion.

Many thanks to Sanli for reading my thesis and helping me during the daily lab life: I learned many things during your short explanations.

Many thanks to all the people in the Ornstein-prisonlab with whom I had good conversations and funny times.

In the end, thanks to all the friends from everywhere who were by my side, concretely or by telephone, during the last $\sim$ 8 months.
Thanks to my sister, my family, IV and my relatives for pushing me towards roads that are unknown to me and to them, too.

# Contents

*To Evey for her patience while waiting for me to go out. . .*

# Chapter 1

# Introduction

Scattering has been given an increasing attention by scientists in the last decades and the trend is still growing. In fact, a scattering process happens each time that particles or waves deviate from their original trajectory: it is one very fundamental process.

Scattering media is a term used to designate all those materials which scatter more than absorb light: in case of strong absorption, most of the radiation is absorbed. In the case of multiple scattering, the light field is scrambled but information is still in the scrambled image that we see: by knowing the ingoing beam we can retrieve the interaction with the scatterer.
When coherent light is sent on such a material, it gives rise to speckle patterns: **speckles** are an effect of the mutual interference of many waves, each one corresponding to a different channel of the back surface of the scatterer. In fact, each position on the back surface is a channel of the scatterer; by looking at speckles, we look at the average far field. This knowledge together with many degrees of freedom over the beam's shape allow to control where the interference is constructive.

In this thesis we want to look *behind* a scattering layer: to achieve this, we create an intensity-enhanced focus and scan it around. The intensity-enhanced focus is used to increase the contrast and the sharpness of the image, and the motion is used to retrieve the object's shape.

Focus is generated by means of **wavefront shaping** [1] [2] [3] [4]: this class of techniques permits to modify the shape of the wavefront before sending it through the scattering layer.
Motion, instead, is achieved by exploiting the **optical memory effect** [5] [6] [7]: for reasonably small angle, a tilt of the beam on the layer's front surface correspond to a tilt of the beam on the back surface. This allows us to move the focus.

With the use of a *Spatial Light Modulator* [8] we have reached enhancement of in-focus intensity between 10 and 1000. We describe how the use of an initial uniformly distributed random wavefront allows us to reach high-enough

pre-enhancement.
However, it is still unclear why, also with the use of the same scatterer, the range of enhancement is so large.

Although our initial plan was to compare two imaging techniques in reflection, because of time, we could not implement them. So, this thesis is about creating a focus with high enhancement behind a scattering layer and scanning the previously created focus around by means of the memory effect.

To conclude, better knowledge of the processes described above could eventually lead to image inside human tissues with properly modulated visible light. In addition, as pointed out later in the thesis, the focus is a property of a lens: thus, being able to create a focus behind any material means that we are using such a material as a lens.

## 1.1 Information on the project

Usually, a thesis project in the Experimental Physics master's program is worth 60 ECs corresponding to one year of research. Instead, the thesis project reported in this document is worth 45 ECs: next semester, I am going to follow the Educational Profile which reduces of 15 ECs the full amount of credits available for a master's thesis.

## 1.2 Outline

In chapter 2 we give information on theory: topics are scattering, memory effect and imaging through scattering media. In addition, we show our experimental method and compare with some literature.

In chapter 3 our experimental apparatus and its working way is described in detail.

In chapter 4 the preparation and the measurements performed are explained.

In chapter 5 we report the results obtained in detail.

In chapter 6 we write our conclusions and (possible) future research.

# Chapter 2

# Background information and theory

After the creation of radar in the 20th century, it became clear that seeing something is not only feasible with visible light: radars, by using radio waves, actually allow to see objects inside a dense cloud (impenetrable by our sight). Scientists started to wonder whether it could be possible to use visible light to look 'Through walls and around corners' as theoretically explained by Isaac Freund in 1990 [5]: if light passing through a wall is not completely absorbed, we can see something but we need to process information to understand what it is.
If coherent beams pass through scattering media, they get scrambled and give rise to speckle patterns. However, if we are able to reconstruct the paths of light, then we can extract the information messed up by the complex medium, as if we were capable of looking through walls and around corners.

While in the past, multiple scattering - when light scatters many times before being recorded - was 'usually seen as an impediment to focusing and imaging' [2], now it is an active field of research with many different applications. For example, it may eventually lead to seeing through human tissues without using dangerous radiation (such as X-rays), but by using a properly modulated visible laser beam and, in addition, to find other imaging techniques which use many different materials as lenses.

## 2.1 Scattering

Scattering is a physical process in which radiation or particles are forced to change their original trajectory of propagation because of interaction with some localized non-uniformities. Non-uniformities, called scatterers, can be of many different types: particles, molecules, droplets, density fluctuations,

impurities and/or inhomogeneities in a crystalline solids, just to name some. In addition, sizes of scatterers vary widely: from less than a nanometer for gas molecules to some millimeters for water droplets.

There are three main types of scattering:

- *elastic scattering*: the frequency of the incident light is the same as the scattered light (e.g. Rayleigh and Mie scattering).
- *inelastic scattering*: the emitted light has a wavelength different from the incident light (e.g. fluorescence and Raman scattering).
- *quasi-elastic scattering*: the frequency of the scattered light shifts (e.g. Doppler shift due to moving matter).

Scattering can be either a one-time event (single scattering) or radiation can hit the scatterers many times (multi scattering): there is an in-between range where light scatters some (but not many) times.
Single scattering is dominant in optically thin media and in strongly absorbing media. In optically thin media, it is more probable to exit the medium than scatter again. In strongly absorbing media, it is more likely to be absorbed than scatter again.

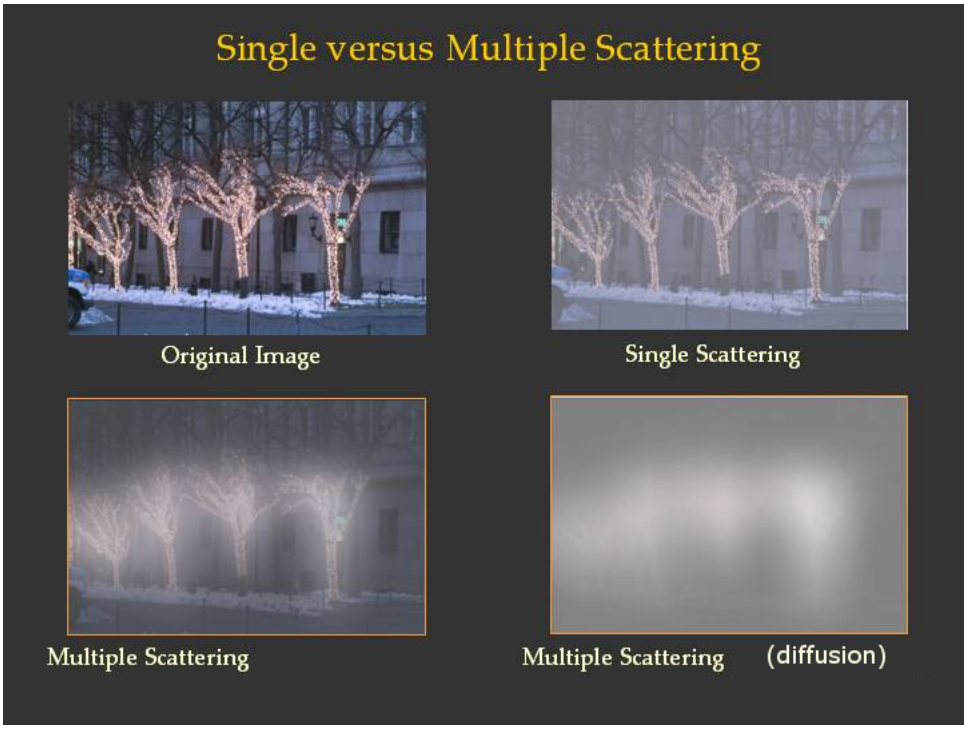


FIGURE 2.1: Visualization of different scattering regimes: top to bottom and left to right, the number of times that incoherent light has scattered increases. [9]

Figure 2.1 shows scattering simply by adding different effects to a photograph: 'This picture shows the results of adding weather effects to photographs[...]', effects which are obtained by simulated Monte Carlo methods of a scattering model [9]. By going from top to bottom and from left to right, we see incoherent light that scattered respectively zero, one, more than one, many more times. The bottom pictures are an example of diffusive regime: diffusion comes from a Latin word, *diffundere*, which means 'to spread way out'. If you start with a dense bulk of solute inside of a solvent, what happens is that the more one waits, the more diffusion brings the system towards a total homogeneous situation (e.g. salt and water: after a while the salt is mixed and the bulk introduced at beginning is disappearing.). As one can see, the left picture is a very blurred real photograph, corresponding to a 'finite amount' of diffusion, while the right one is almost unrecognizable, corresponding to total homogeneity.
Thus, no scattering, no blur, few scatterings, small amount of blur and the more scattering, the more homogeneous is the image: in the last case, initial information is completely scrambled.

Scattering theory successfully explains the formation of a rainbow (interaction of light waves with droplets of water) as well as the passage of a laser through a piece of biological tissue. Although these processes seem completely unrelated, they share the same mathematics: they are solutions of partial differential equation 2.1, which propagated freely 'before', came together and interacted, and then propagated away 'after'.
We limit our study to electromagnetic waves.

If polarization is neglected, electromagnetic waves are described by the Helmholtz equation:

$$\nabla^2\Psi(\mathbf{r},t) = \frac{n^2(\mathbf{r})}{c^2}\frac{\partial^2\Psi(\mathbf{r},t)}{\partial t^2}, \tag{2.1}$$

where $\Psi$ is the wave function, c the speed of light and n the refractive index. Equation 2.1 is linear and symmetric in space and time, meaning that a solution is the same if t $\rightarrow$ -t and $\mathbf{r} \rightarrow$ -$\mathbf{r}$ and that a linear combination of two solutions is still solution to the equation. The symmetry is broken if n($\mathbf{r}$) = f($\Psi$), that means that the refractive index depends on the wavefunction itself: this is not our case.
Inhomogeneities of the medium are coded into the refractive index n($\mathbf{r}$) which it is the only term related to the medium in equation 2.1.

Usually, scattering is described with distributions that depend on the particles' or waves' mass, on the angle, on the momentum, on the wavelength: an impact can depend on many properties. Nevertheless, multiple scattering is usually deterministic when we consider the interaction with one very specimen: because of the many interactions, randomness is averaged out and only some channels stay open. We are going to exploit the determinism due to multiple scattering.

To conclude, scattering is an active field of research at the moment because it helps understanding interactions between light and small objects. The direct scattering problem is the determination of the scattered probability distribution from the scatterer's properties. Vice versa, the inverse scattering problem is the determination of the scatterer's properties based on the scattered probability distribution.

### 2.1.1 Speckles

Figure 2.2 shows an example of speckle pattern: yellow spots represent constructive interference while blue destructive. X and Y axis represent the camera axes and each pixel shows intensity as a number in the range $(0,255)$.
By imaging a laser beam that passes through a scattering material, we see a well-defined speckle pattern.

Parameters governing scattering are the wavelength of light, size, shape and refractive index of the scatterers and the refractive index of the surrounding medium.

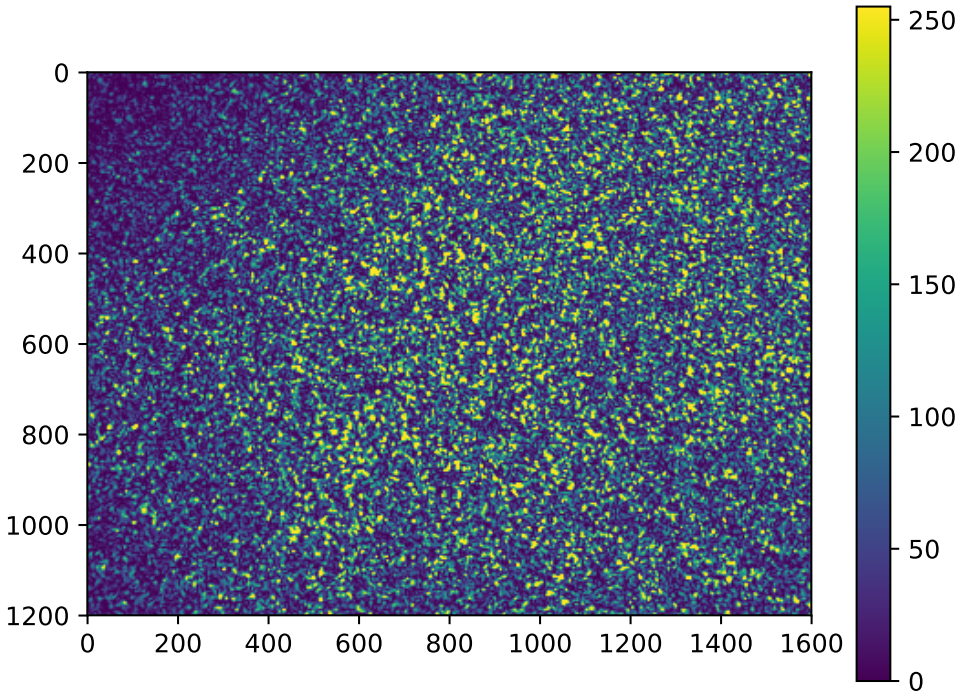


FIGURE 2.2: Speckle pattern obtained with plastic scattering layer and 532 Hz laser. On the right side, the color bar is shown.

When coherent light impinges on a scattering medium, it generates patterns called *speckle patterns*.
This phenomenon is common when a coherent source of light encounters a material with many scattering particles: for example a rough glass surface, some pigments in paint, dust, a turbid liquid and paper. When a coherent source of light, illuminates such a material, each scattering point behaves as source of secondary spherical waves: their mutual interference gives rise to such specific patterns informally called speckles.
On the other hand, for incoherent light, non-polarized and non-monochromatic light, this results in blurring as in figure 2.1. This is due to a simple fact: different wavelengths give different speckle patterns and, as result, individual patterns are averaged out. As in last figure of 2.1 we do not see any clear pattern and the figure is blurred.

As one can see in figure 2.2, speckles are, at eye-sight, a pretty random pattern.
However, each set of illumination patterns and associated speckle patterns is unique for a scattering material. It can though be sensitive to ambient conditions such as temperature or humidity: it is very hard to be 'under same conditions'.

So, *speckles* are induced by the interference of many waves of same wavelength and different phase and amplitude.

### 2.1.2 Medium

To generate and use speckles we need a coherent source and a scattering layer or a diffuser: we cannot use all materials.

The mean free path of a material is the average length traveled between collisions or scattering events.

Speckle patterns can appear if, for instance, we use a material that has a very short mean free path or if we use a very thin layer of large-mean-free-path material.
Media that can be used for our experiment are non-completely opaque and non-completely transparent: for example thin layers of paper or tape, plastic, diffuser.
If the medium had a really large mean free path, light would just pass through as if the medium was completely transparent.
On the other hand, if the medium were completely opaque, by definition electromagnetic waves could not pass through it meaning a mean free path close to zero: light is mostly absorbed in this case. We do not need such materials.

Thin layers that we can use are, for example, made of titanium dioxide, gallium phosphide, tape, plastic, paper and biological materials.
In this work, we use a plastic scattering layer and a glass diffuser: although differently specified, results are obtained with the plastic layer.

## 2.2 Memory effect

A speckle pattern is a scattering-layer-specific mark [6] of a complex medium. Tilting the beam on the front-surface of the medium results in a tilt of the beam on the back-surface, which results in a shift of the speckle pattern in the far field: this is called **optical memory effect** and it is valid for small angles.

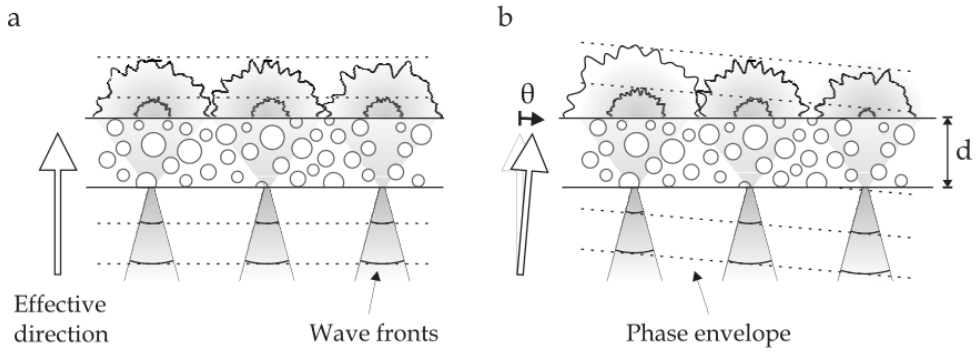


FIGURE 2.3: Schematic picture explaining the optical memory effect of scattered light in transmission. **a**: An array of spots that are imaged onto the surface of a disordered slab with thickness d. The spots are separated by a distance that is larger than the sample thickness and arrive with equal face at the surface of the slab. In transmission a complex field pattern arises from three independent areas. The dotted lines denote the baseline phase envelope. **b**: The relative phase between the three spots is changed to resemble a tilt $\theta$ of the phase envelope. As the relative phase of each of the transmission areas is directly related to the phase of the spot from which it emerges, the transmitted light encounters the same relative phase change.
Figure and caption from [10].

Each scattering layer gives rise to a well-defined speckle pattern, and tilting the beam, for small angles, has the same effect as linearly changing the phase of the ingoing beam on the surface of the medium, as can be seen in figure 2.3 b. When a large phase variation occurs on a length similar to the thickness of the medium, the speckle changes. Vice versa, if the phase variation is small enough (compared to the thickness), the speckle pattern is shifted while remaining unchanged.

Quantitatively, tilting is possible until the so called memory effect angle: from [11], 'the angle at which the focus intensity has decreased by a factor e is $\sim \frac{\lambda}{2\pi d}$', where $\lambda$ is the wavelength of the ingoing wavefront and d the thickness of the medium.
The maximum shift in pattern is proportional to

$$\Delta x \propto L\Delta\theta = \frac{\lambda L}{d}, \tag{2.2}$$

where L represents the distance of the focus from the back surface of the scattering layer.

Recently, a generalized model for the optical memory effect has been studied in [7].
The optical memory effect predicts that a tilt of the ingoing beam produces a tilt of the wavefront scattered by a thin layer. It has been shown [7] that, in anisotropically scattering media, a shift in the ingoing beam produces a shift in the scattered wavefront, as in figure 2.4: in biomedical imaging it could be implemented to physically shift a focal spot previously formed deep inside a tissue by translating an incident optical beam.
To conclude, both the effects are 'manifestations of one and the same general source of correlation within a scattering process, which depends upon how an incident wavefront is both tilted and shifted' ([7]).

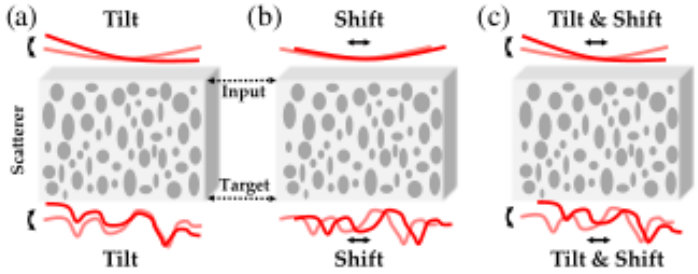


FIGURE 2.4: Three different types of spatial correlations in disordered media. (a) The optical "tilt" memory effect [6], where an input wavefront tilt leads to a tilt at the target plane. (b) The anisotropic "shift" memory effect [9], where an input wavefront shift also shifts the target plane wavefront. (c) Our new generalized memory effect, relying on both tilts and shifts, can maximize correlations along the target plane for a maximum imaging/focus scanning area.
Figure and caption from [7]

## 2.3 Imaging through scattering media

The aim of the project is imaging through scattering media. Imaging is performed in the following way: a focus is created behind a scattering layer and, then, scanned by means of memory effect; the reflected light is measured and used to reconstruct the image.
In this section, I describe the ingredients needed to look behind a scattering layer.

### 2.3.1 Transmission matrix

Transmission matrix (TM) features the transfer function of a complex medium [12]: in the case of scattering media, scattering properties of the material are coded into the TM.

Equation 2.3 is the simplest way to describe the problem we want to solve

$$|out\rangle = \mathbf{T}\,|in\rangle\,, \tag{2.3}$$

where $|out\rangle$, represented as a vector in a suitable space, is the outgoing beam, $|in\rangle$ the ingoing beam and $\mathbf{T}$ is the Transmission Matrix (TM) of the system.

As can be seen in figure 2.5, a lens can be described by a well-defined transfer function coded in a simple TM; instead every sugar lump has a unique random TM.

Thus, if we knew the TM of the system, we could numerically calculate the best wavefront to achieve the desired result: focusing through our scattering layer.
This is not the usual case: we need to find the components of the TM needed to create a focus behind the scattering layer. In order to find them, two different approaches have been developed. TM methods measure the TM of the system in advance, find the vector(s) to maximize selected channels and then modulate the wavefront. On the other hand, iterative methods update the wavefront while maximizing the selected channels.
The TM, however, is not *a priori* known.

Some related work has shown that, by increasing the optimization area on the transmission side, the total transmitted intensity is enhanced while the total reflected intensity decreases, as studied in [13] and in [3] by the group of prof. Willem Vos. In addition, it has been numerically calculated how absorption modifies maximal transmission and minimal reflection channels in a 2D waveguide [14]: when absorption is strong, all paths where light

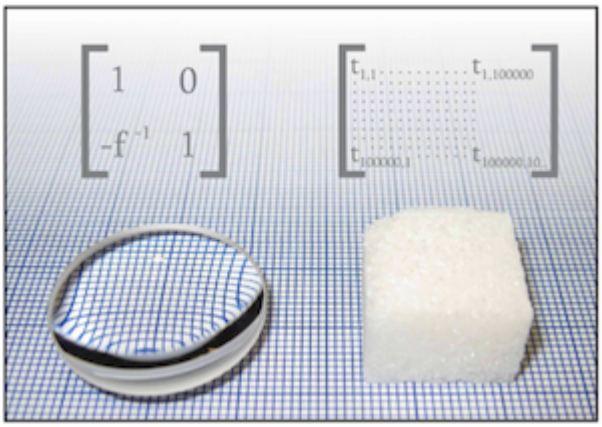


FIGURE 2.5: Two optical elements fully characterized by their transmission matrix, which relates the incident wave front to the transmitted one. In the case of a thin lens, the transformation of the wave front is described by a $2x2$ matrix operating on a vector describing the wave front curvature. For more complex elements such as a sugar cube the transmission matrix operates in a basis of transversal modes, which is very large. Full knowledge of the transmission matrix enables disordered materials to focus light as lenses.
Figure and caption from [10].

scattered many times are suppressed, and only ballistic light remains. Thus, by an increase in absorption, the system passes from diffusive regime to ballistic-like transport meaning that light only goes through non-scattering or single-scattering trajectories while multi-scattering trajectories are 'closed' by absorption.

### 2.3.2 Wavefront shaping

Wavefront shaping is a category of methods used in many applications such as beamers, screens and, since some years, in different areas ranging from fundamental research in Physics to medical imaging.
Adaptive Optics include all techniques used to correct distortions in optical systems: in particular wavefront shaping refers to techniques used to modify the wavefront shape.

We want to use wavefront shaping to solve our problem.
As one can see, there are three variables in equation 2.3: we need to know two variables in order to find a solution. Although **T** is constant, it is not *a priori* known.
The input can be controlled, for example, through a Digital Micromirror Device (DMD) or through a Spatial Light Modulator (SLM): these devices allow to control many degrees of freedom in the laser beam.

We also know the output that we want to obtain, a small focus in our experiment.
To see the created focus, we need to place a detector behind the scattering layer and in some situation this can be very hard.

By wavefront shaping we aim to find the input beam that maximizes a selected output mode. This means measuring the row of the TM corresponding to a focus as output. This can be done by scanning all input channels and by choosing the relative phase which make the intensity in the desired focus increase: in-focus constructive interference is our goal. When dealing with strongly scattering materials, the maximum achievable enhancement is

$$\eta = \alpha(N-1)+1, \tag{2.4}$$

where N is the number of independently controlled channels and $\alpha$ is $\pi/4$ for phase modulation only, $(1/2\pi)$ for intensity modulation only and 1 for both [15].
Typical values of enhancement in other works are in the order of 10 to $10^3$, depending on the stability of the scattering layer and the number of controlled channels.In the next subsection, I am going to describe some algorithms and how they actually work.

### 2.3.3 Focusing algorithms

We divide the SLM into groups of pixels that we call SuperPixels (SP). Each SP represents a degree of freedom of our input beam.
The maximum number of SPs that we can choose is equal to the total number of pixels of the SLM but this does not give us the best results due to a low signal to noise. There is an optimal value for the number of SPs used to optimize our system in different moments of the optimization process.
In addition, we only select the region of the SLM where the beam actually impinges on: this means only testing and using a circular area on the SLM.
Three algorithms are described: stepwise sequential algorithm, continuous sequential algorithm and partitioning algorithm.

The *stepwise sequential algorithm* tests the phases on one independently controllable channel and chooses the one that results in highest in-focus intensity. The chosen phase is stored and, after all channels are tested, the SLM is updated with the focusing wavefront. The working scheme is depicted in figure 2.6 **a**.

The *continuous sequential algorithm*, in figure 2.6 **b**, differs from the stepwise sequential algorithm for one only operation: the wavefront is updated on the SLM every time that the best phase for one channel is chosen (instead

of updating only once, at the end of the operation). This makes background intensity and SNR increase quicker than the stepwise sequential algorithm.

Besides these two algorithms, there is an interesting third way to implement the feedback-based wavefront shaping: it is called *random partitioning algorithm*. Two partitions of the SLM are randomly chosen and their relative phase is varied to enhance focus in intensity, then two other random partitions are optimized, and so on, *ad libitum*. In figure 2.6 **c**, it is better described how it works.

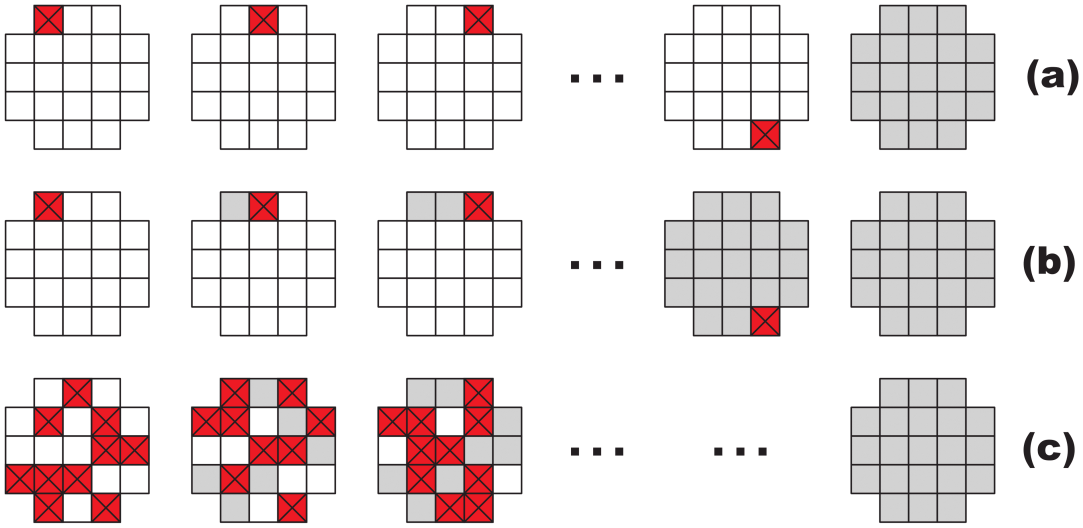


FIGURE 2.6: Principle used in the three different optimization algorithms. (a) For the stepwise sequential algorithm, all segments are addressed sequentially (marked squares). After the optimal phase is measured for all segments, the modulator is updated to construct the optimal wavefront (light gray squares). (b) The continuous sequential algorithm is equal to the first algorithm, except that the modulator is updated after each iteration. (c) The partitioning algorithm randomly selects half of the segments and adjusts their overall phase. The modulator is updated after each measurement.
Figure and caption from [16]

The continuous sequential algorithm is considered the best performing one [15] because it reaches the best optimization faster than the others; moreover, the background is continuously updated so that subsequent SPs are related to the updated background: this is different from the stepwise sequential algorithm which measures the best phase for each superpixel first and then set everything to its best value.
On the other hand, the stepwise method is the most robust because parameters of the apparatus are changed only before and after the optimization process. In this way, it is the easier to understand what is going on during the experiment because every parameter is set and stored not during the actual process of testing and creating the wavefront to get an intensity-enhanced focus.

Thus, if we set our parameters around the 'best' ones, we can use the stepwise sequential algorithm and obtain satisfying enhancements.
However, partitioning algorithm seems to outperform stepwise algorithms in optimizing intensity on a large area [3].

## 2.4 Imaging method

The imaging method is composed of the following steps.

First, a focus is created with the use of wavefront shaping: the focus is positioned on the object plane, which is slightly - $\approx 3$ mm - behind the scattering layer/diffuser. To achieve an intensity-enhanced focus, different portions of the beam are given different phase shifts, through the SLM, so that the result is constructive interference on the focus spot.
Second, the focus is scanned around many times by use of the memory effect.

Third, for every scanned position of the focus, light back-reflected through the scattering layer is measured in two situations: with and without object. This way, the subtraction of the two images results in the object information only. In addition, the back-reflected light is selected in two ways. A 'bucket' detector saving the total intensity, the intensity coming from all the beam, is compared with a confocal technique where only light arriving from specific angles is collected: in figure 2.7 both techniques are schematically shown. We use photodiodes to measure differences in intensity as differences in current.

The *'bucket' detector technique* is very simple.
By wavefront shaping, a focus on the object plane is created: focus means a brighter spot with much darker background. The object is then imaged through light that has been reflected by the object itself and has traveled backward again from the scattering layer: this information is processed together with the applied phase shift, that is the pattern on the SLM, and we can thus retrieve an image of the object.
Nevertheless, contrast is not high because also light coming from the background is reflected and collected in the image.

On the other hand, the *confocal technique*, as the name tells, makes use of a pinhole: a pinhole is used to remove most of the background light and to gather light only from a small portion of the object plane.
The in-focus-contrast of the measurements is expected to increase because of the removal of most of signal due to background.
This is done through a photodiode which is placed behind the SLM: light that did not interact with the object has ideally a flat wavefront because light is back-reflected again through the SLM.

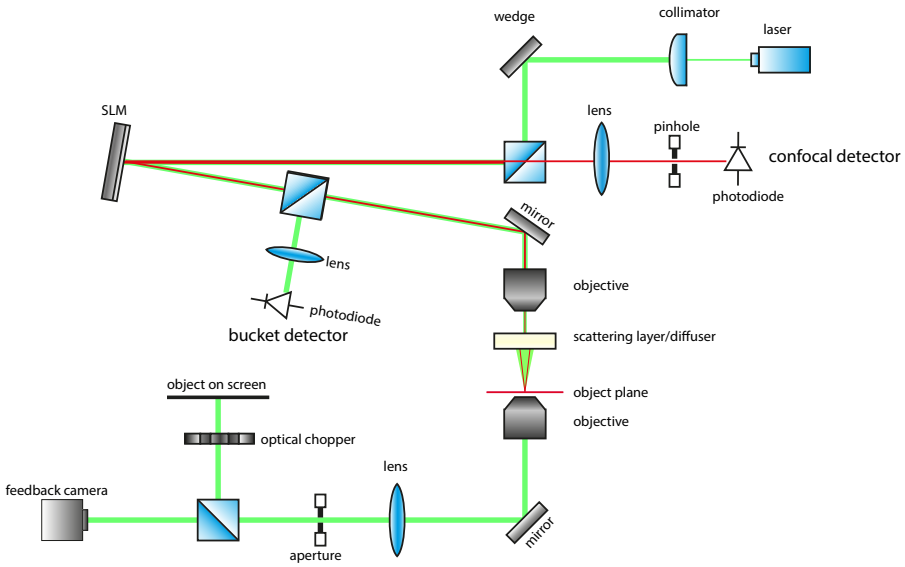


FIGURE 2.7: Schematic of the apparatus with shown positions of photodiodes for the 'bucket detector' and the confocal techniques.

It is also possible to image in transmission. For instance, instead of using a screen as a virtual object and looking at light in reflection, we can use a camera with a pinhole: the pinhole replaces the object and the camera measure the **transmitted** intensity. While the pinhole is projected to the object plane, the camera can record intensities: we can measure contrast and enhancement on the object itself. In addition, we measure changes in intensity while scanning the focus.

## 2.5 Some literature and comparisons

In this section, motivations and works in the field of wavefront shaping and imaging beyond the diffraction limit are presented.

Conventional optical lenses can resolve up to the diffraction limit, approximately 200 nm. Unfortunately, this is not sufficient to see essential structures with sizes of 100 nm such as cellular organelles and some nanoelectronics and photonics components.

To enhance the resolution, many techniques still rely on beams that propagate straight by rejecting light which has been scattered more than few times: two examples are optical coherence tomography [17] and multiphoton microscopy [18]; in the first case a reference beam is used while, in the second,

photons with low (enough) energy are not taken in account.
Fluorescent based methods are used to improve the resolution that, unfortunately, depends on the optical focus shape which is created through conventional lenses. In addition, it is not always easy to bind specimen and fluorescent dye.
Near field microscopy for example brings 'nanosized scanning probes or even antennas' very close to the object and detects the evanescent field. However, when we need to image turbid media or biological tissue, light undergoes multiple scattering events: then the medium does not absorb much, almost all information is still in the speckle pattern and just needs to be retrieved [19] [15].

Wavefront shaping is a technique used also to enhance resolution: to achieve good wavefront shaping we need to have feedback for the system.
The main drawback of feedback-based methods is the very need of a feedback signal: this can be obtained by placing a camera behind the scattering layer. Nevertheless, recently some groups have used combinations of optical (ie fluorescence) and acoustic waves (i.e. photo-acoustic) to characterize with good precision some Transmission Matrix (TM) [20].
In another example, a Spatial Light Modulator and full-field interferometric measurements on the camera allow to experimentally retrieve the components of the TM of different complex media [21].
By the combination of wavefront shaping, a scattering layer and a fluorescent probe, it becomes possible to image an object behind an 'opaque layer that scatters all incident light' so that there is no need to place a camera behind the scattering layer [1].

The HIRES technique (High-Index Resolution Enhancement by Scattering) makes use of 'a slab of high-index material (GaP) on top of a strongly disordered scattering layer' to focus light which had already a shaped wavefront [4].
Because of the strongly disordered layer, light undergoes multiple scattering events which enable to couple it to all angles of the high-index material. By wavefront shaping the ingoing beam, an optical focus is created on the object plane and scanned around by use of the optical memory effect: this can be done both by tilting the beam and by changing the phase through a SLM [4]. One major problem was internal reflection solved with an anti-internal-reflection coating.
A resolution of $97 \pm 2$ nm is achieved, furthermore this method has been shown robust against aberrations or surface roughness because of its intrinsic random nature (the inherently random paths followed by light waves).

# Chapter 3

# Experimental Setup

In this chapter, the experimental apparatus is described.
Topics of the sections are how the setup is supposed to work, laser and stability check, optical components, SLM and SLM calibration, scattering layer/diffuser and used software.

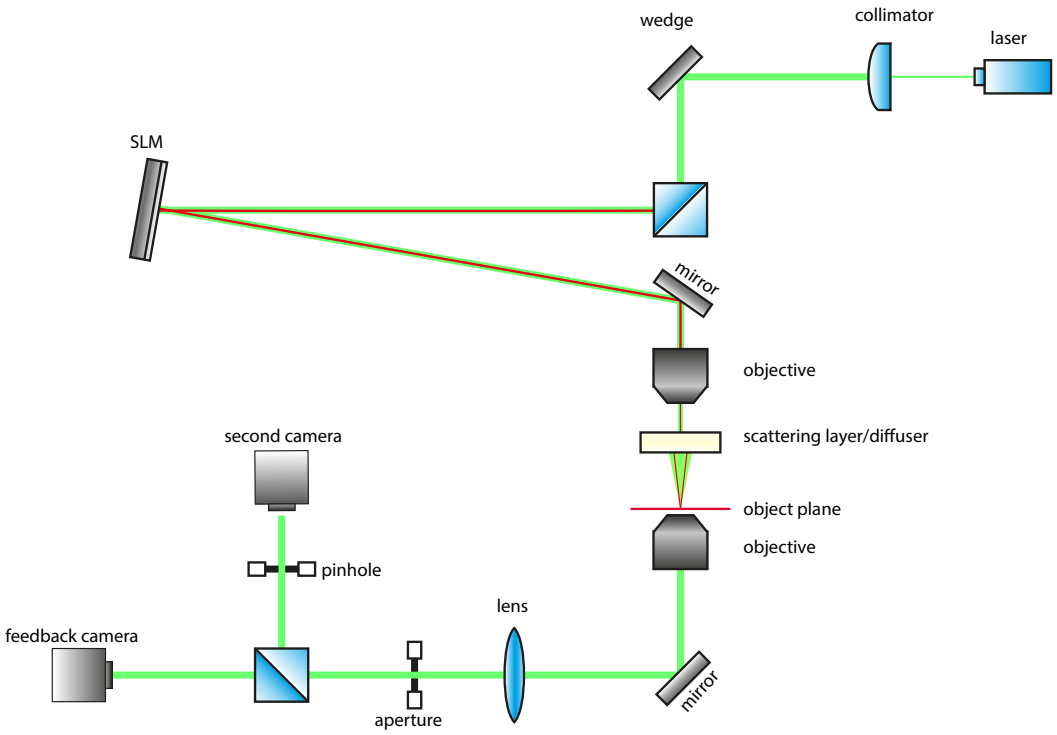


FIGURE 3.1: Schematic of built experimental setup: the real object on a screen is replaced by a pinhole at same position. A camera behind this pinhole allows to retrieve transmitted intensity on the object.

## 3.1 Ideal setup operating mode

Figure 3.1 shows the schematic of my experimental setup[1].

It is composed of the laser, two cameras, some optical component such as collimator, mirrors, beam splitters (BS), objectives, glass wedge, optical chopper and the spatial light modulator (SLM).

Laser light is coupled through a fiber to the experimental apparatus. First a collimator is used to expand the beam and make it collimated, then a wedge takes away around $90 - 95\%$ of incoming power: thus we can use the laser in its best stability regime - between 50% and 100% of maximum value - and still have low enough power on the scattering layer.
The SLM is used to wavefront-shape the beam profile. After, there is an objective, the scattering layer and another objective: the first objective is used to Fourier transform the SLM onto the surface of the scattering layer while the second objective is used, together with a lens, to image the object plane on the so-called feedback camera. The feedback camera is used during the optimization process to detect whether the in-focus intensity increases by changing the wavefront of the beam.
The BS in between the two cameras is used to generate a virtual object in the object plane: the space between objectives and scattering layer is very small and it is very hard to make place for an object to be imaged. This will be exploited by projecting an object in the virtual plane to the object plane.

## 3.2 Laser

The laser we are using is a Coherent OBIS 532 nm CW (Green) fiber coupled laser [22]. The maximum power is 120 mW. We use it in the power range 50% - 100% of the maximum power.

In the next subsection, laser stability is performed: these measurements were performed to understand why it was initially impossible for me to create a focus through a scattering layer using wavefront shaping. To understand effects caused by the stability of the laser, we checked fluctuations/correlations of the laser.

[1] A real photo of the setup is visible in the appendix.

### 3.2.1 Laser stability

We performed stability checks at 1 mW and at 50 mW by means of correlations at different time scales: if correlation is too low, probably the laser does not work properly or is too unstable.
That is not the case. Our laser is working properly and the best stability regime found is at 50 mW.

Correlation is calculated by multiplying the value of the same pixels for different frames and normalizing it as in the following equation:

$$C(t) = \frac{\sum_{x,y} I(x,y,t)I(x,y,t_0)}{\sqrt{\sum_{x,y} I^2(x,y,t)I^2(x,y,t_0)}}, \tag{3.1}$$

where $I$ represents intensity related to pixel $(x,y)$ at time $t$ and $t_0$ represents the initial time.

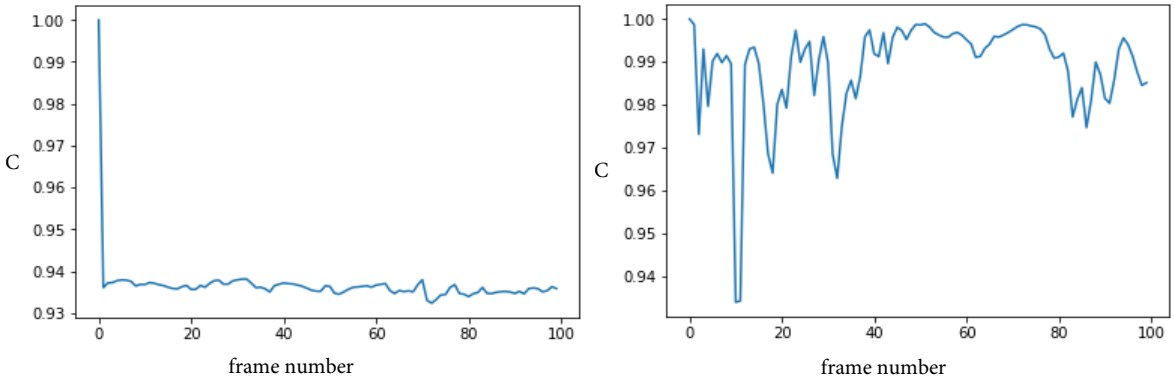


(A) 1 mW short time correlation.

(B) 50 mW short time correlation.

FIGURE 3.2: In this figure, the short time correlation C, as in formula 3.1, is plotted with the number of frame: every 0.1 s, a frame is saved and correlation is calculated with the first frame. (A) shows correlations for laser at 1 mW power and (B) at 50 mW.

The difference between short and long scale correlation is the time in between two different frames. For long scale correlation, an image is recorded every 2 seconds while, for short scale correlation, at the fastest system speed. Then, correlation between first and current (Nth) frame is calculated and plotted with respect to N. As can be seen in Figures 3.2 and 3.3, short scale correlation is much higher when we use 50 mW (to notice that there is only one peak below 0.94 and correlation elsewhere is between 0.96 and 1). On the other hand, long scale correlation shows a similar trend with different powers.

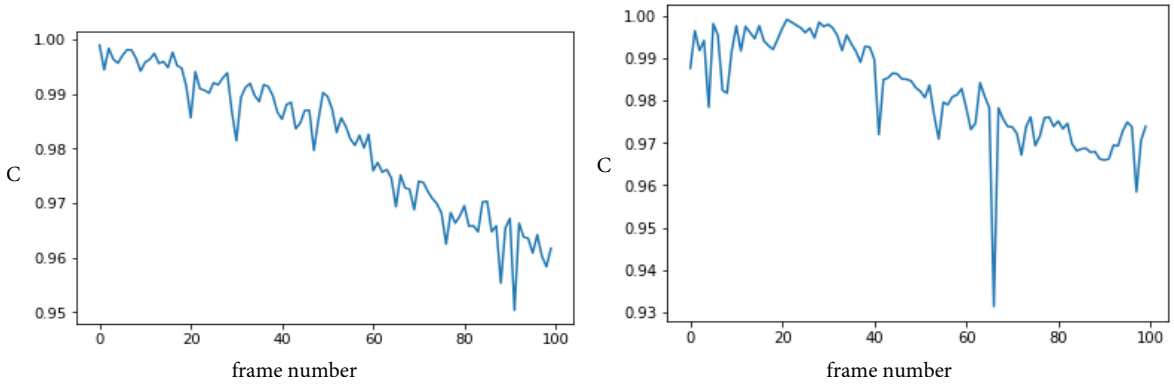


(A) 1 mW long time correlation (B) 50 mW long time correlation

FIGURE 3.3: In this figure, the long time correlation C, as in formula 3.1, is plotted with the number of frame: every 2 s, a frame is saved and correlation is calculated with the first frame. (A) shows correlations for laser at 1 mW power and (B) at 50 mW.

## 3.3 Optical components

BSs and mirrors are used to align and split the beam. In addition, a glass wedge is introduced to reflect out of the system most of the power so that, using the laser in range $60 - 120$ mW, it will be possible to impinge on the scattering layer with (only) $\sim 1$ mW. Objectives are Olympus $10x$, $FN22$ with 0.25 NA.

The optical chopper, shown in 2.4, is used to periodically block the light projecting the real object on the object plane: if the chopper blocks the object, no light is reflected and we measure all the other reflected light; if it does not block, we also measure the signal reflected from the object. Now, by subtracting the two measurements, we can look at the signal from the object only.

The cameras used are both Basler dart daA1600 $-$ 60 $\mu$m. The feedback camera is used for the optimization process to create and move the focus. The second camera has been used both for calibration of the SLM and, in combination with a pinhole of 50 $\mu$m, to read the transmitted intensity on the 'object': in this case, the object is a 50 $\mu$m pinhole which is projected on the object plane through the second objective.

## 3.4 SLM

A SLM is a device used to modulate amplitude, phase or polarization of light waves.

It typically uses a reflective liquid crystal microdisplay (LCoS - Liquid Crystal on Silicon). A layer of liquid crystals on top of a silicon wafer is controlled by electricity: different voltages correspond to different average orientations of the LC molecules for phase and/or amplitude modulation. In our case, the SLM is a phase-modulation only device. In addition, the voltage is periodically reversed and this causes noise. In practice, the software uses a gray scale (0 to 255) to control the voltage which decides the liquid crystals' orientation.

We are using a Spatial Light Modulator called PLUTO 1 from Holoeye [23]. PLUTO 1 has 1920x1080 pixels with a 'pixel pitch' of 8 $\mu$m. It has a reflectivity of around 65% and a diffraction efficiency of more than 80%.

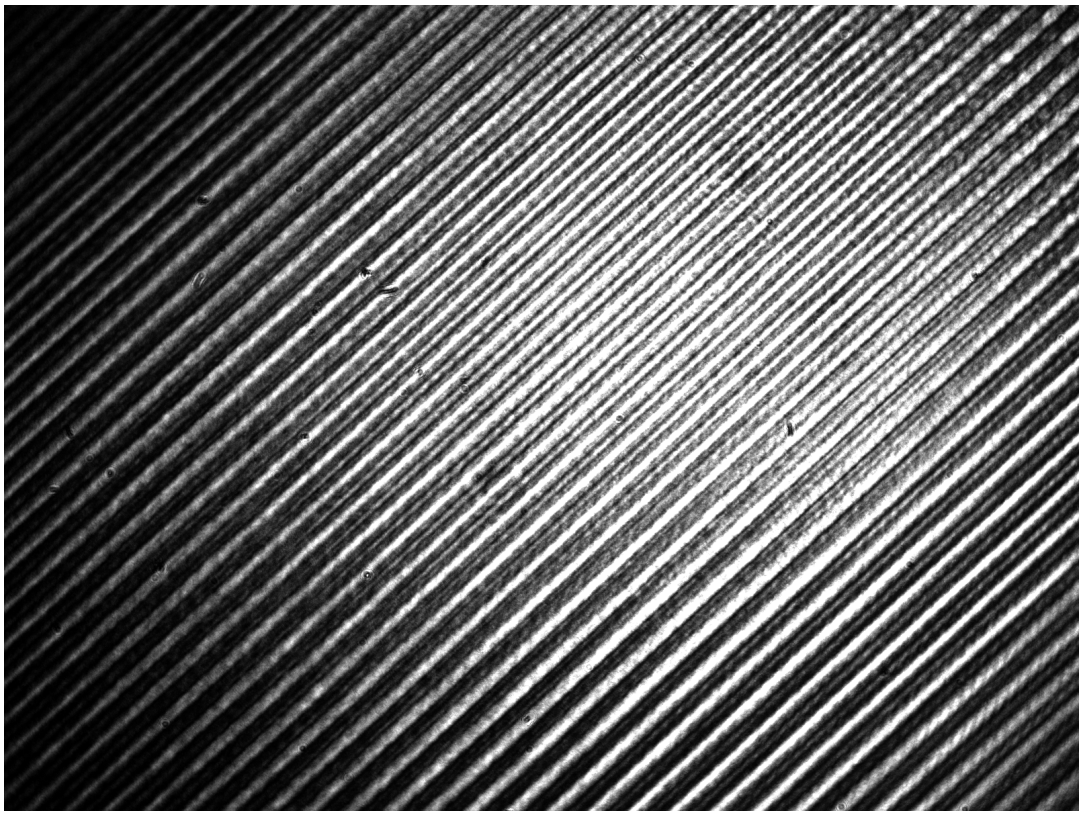

FIGURE 3.4: We update the SLM with a step diffraction grating and take an image with the feedback camera. The grating is visible because of non-ideal imaging configuration: in fact, the SLM is phase-modulation only.

The SLM is read by the computer as a secondary screen and refreshed at 60 Hz frequency; to make sure that a photo is taken only after (or before) the SLM is updated, our camera is synchronized to the SLM refresh cycle: a cable connects camera and SLM and carries the triggering signal.

To conclude, in Figure 3.4 one can see a direct image of the SLM when a diffraction grating is applied: vertical lines are updated on the SLM. To understand, the relative orientation of feedback camera and SLM is such that

the lines are diagonal and the camera is (almost) in imaging configuration with respect to the SLM.

### 3.4.1 SLM problems

This test was done before calibration.
If we test the entire gray scale, from 0 to 255 with steps of 51, we expect the intensity in one single small area to vary according to a sinusoidal curve, because gray scale and phase shift (0 to $4.9\pi$ - as stated in [23]) should be linearly related and the speckle is an intensity interference pattern.
However, this is not what I observe when I check, for example, the in-focus intensity fluctuations by varying the phase (i.e. position on the gray scale) of a SP.
We divide my SLM in $60 \times 60 = 3600$ SPs and then save in-focus intensity for every SP. In addition, the phase interval is spanned twice, that means going twice from 0 to 255, to be sure of the boundaries of the gray scale.
So, after updating phase to a SP, I read out and save in-focus intensity. Consequently, we update the SLM with the best phase pattern which is the one that results in the highest in-focus intensity.
Nevertheless, I don't get a significant increase.

As Figure 3.5 shows, in-focus intensity is not at all similar to a sinusoidal curve: in-focus intensity is plotted versus added phase on the SLM for four different SPs. By enumerating SPs as elements of a matrix, this is shown for SP (0,0), (30,10), (50,10) and (30,30). At the moment, the exact reason why everything is going in an unexpected way is unknown. However, if we check the complete matrix of in-focus intensities, we see that around row $17 - 18$ there is no more change in intensity when the phase is varied. This can be seen in the bottom-right picture in Figure 3.5 where intensity is the same for different phases: it seems that the camera is saturated, so that the exposure time of the camera has to be decreased.

### 3.4.2 Calibration of the SLM

We performed a preliminary check to set the laser to linearly vertical polarized beam. This is done to have the best efficiency while modulating the wavefront of the laser beam.

After fixing the laser in position for correct polarization, we calibrated our SLM.
Calibration is done with the purpose of setting the SLM such that we have the larger control on the wavefront phase. Practically, it means that we want to map $(0, 2\pi) \mapsto (0, 255)$.

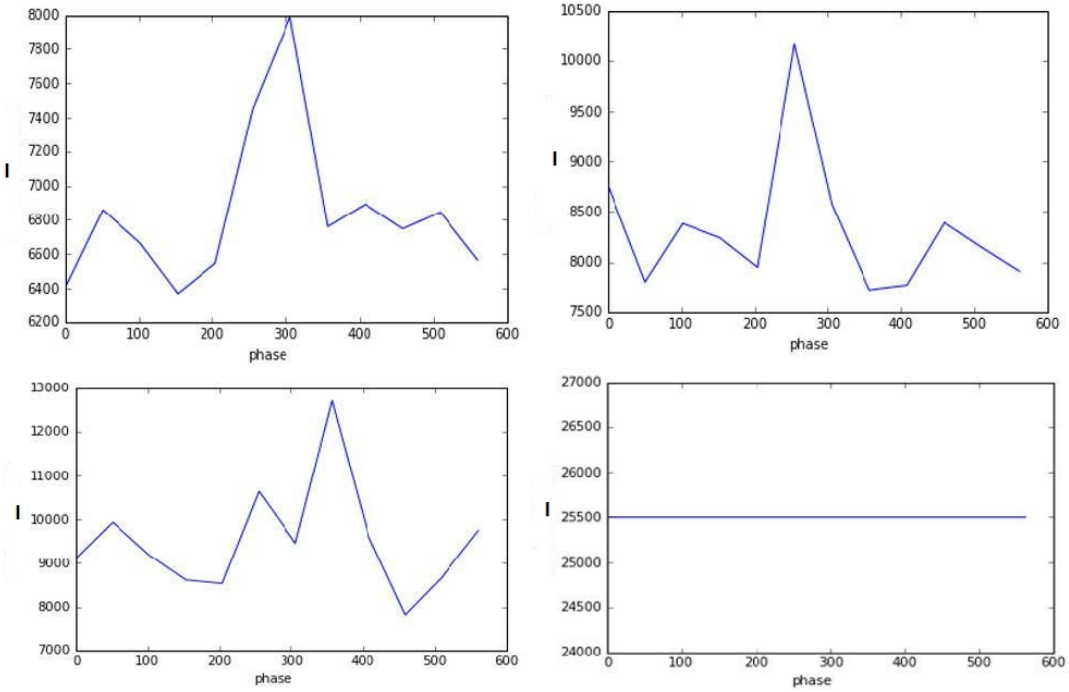


FIGURE 3.5: The in-focus intensity **I** is plotted with the phase added to the superpixel. Every time we span twice the interval $(0, 255)$ corresponding to $(0, 4\pi)$. This is shown for different superpixels: (0,0), (30,10), (50,10), (30,30).

Through *Pluto Configuration Manager*, a control software produced by Holoeye [23], we can change the maximum and minimum voltage of the SLM: these parameters determine the maximum and minimum degree of rotation of the liquid crystals.

On the SLM we generate a step diffraction grating, shown in Figure 3.4. The grating is Fourier transformed through a lens on camera, where the first diffraction order is selected. We measure its intensity while changing the grating depth. One phase is kept at a fixed value while the other spans all range. A $\sin^2$ function is then fit to data: if the error is small, then calibration is obtained and the SLM is now calibrated.

In Figure 3.6 and 3.7 we show the intensity of the first diffraction order as a function of the gray scale values: we modulate the grating depth keeping one value fixed and changing the other.
The curve in Figure 3.6 shows that, before calibrating the SLM, our phase could change between 0 and $\sim 5\pi$: the plot shows intensity, a $\sin^2$ function, so each of the 2 camel humps corresponds to one $2\pi$ period. This means that before calibration we had more than $4\pi$ phase modulation.

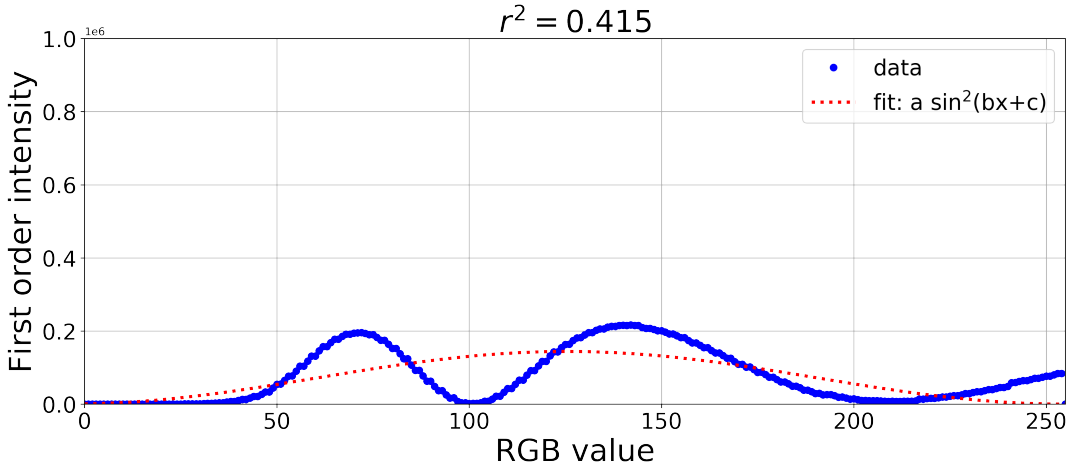


FIGURE 3.6: Intensity of the first diffraction order is plotted with varying diffraction grating depth before calibration.

So, by looking at Figure 3.6, we understand that we need to shrink the voltage interval: this is done in order to decrease the possible rotation of the liquid crystals. Thus, we shrank the interval between maximum and minimum voltage. What we want to see is only one maximum in the curve and a well-covered interval.
By applying in our case respectively 2.34 V and 1.35 V for maximum and minimum voltage, we obtain the following Figure: 3.7.
Calibration is done!

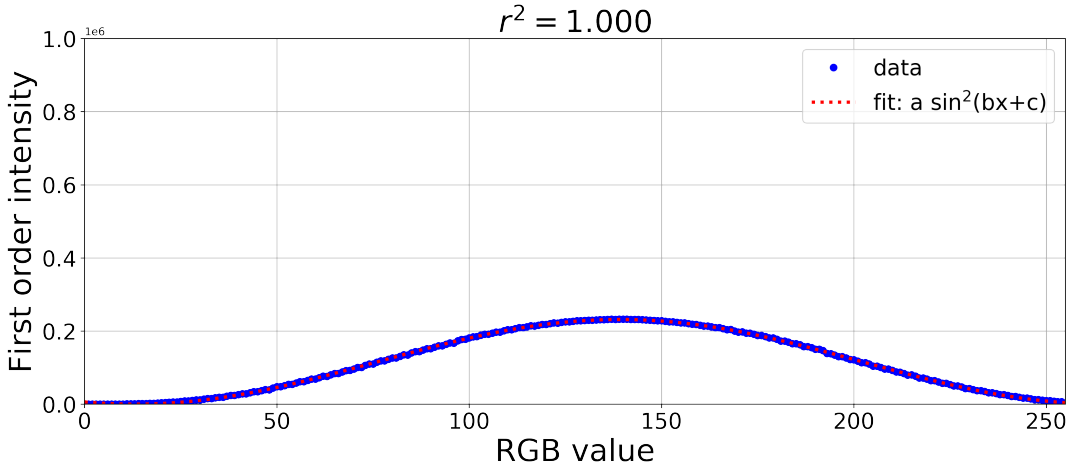


FIGURE 3.7: Intensity of the first diffraction order is plotted with varying diffraction grating depth after calibration.

## 3.5 Scattering layer/diffuser

The scattering layers that we use are a glass diffuser and a thin layer of plastic material: the thickness is less than 55 $\mu m$. The material is optically dense

and composed of very scattering particles, probably titanium dioxide $TiO_2$ but the scattering part is not the full thickness.
The nature of the layer is not actually very important provided that it is not completely transparent, neither completely opaque and strongly scattering. However, each material has slightly different parameters, i.e. number of superpixels and exposure time, to obtain good enhancements.

Strongly scattering materials used for similar experiments are titanium dioxide ($TiO_2$) pigments [19], gallium phosphide ($GaP$) [4] and zinc oxide ($ZnO$). Sometimes, high-refractive-index nanoparticles are used; if such particles are also charged, a multi-focusing lens can be created by mixing them with a liquid and applying different electric fields to change the focal length.

## 3.6 Software

We use are Python with the Anaconda suite and Coherent Connection OBIS.

Coherent Connection is used to set the laser working power.
Python, with libraries slmpy, at [24], and pypylon, at [25], permits to control the SLM and the cameras respectively: this is needed to select the added phase corresponding to largest intensity for the system, otherwise the in-focus intensity cannot be optimized.
Three main algorithms are shown in [15]. We used both stepwise sequential and continuous sequential algorithm although we partly rewrote the code.

# Chapter 4

# Experiment

In this chapter, I describe the steps that are necessary to perform an experiment, the preliminary measures that were done and the experiments that were performed in greater details.

## 4.1 Preparation, alignment, configuration

In this section, all operations necessary to prepare the experiment are described.

First, we want to collimate and align the beam: thus, a collimator and irises (adjustable apertures) are used to make the beam parallel and to force the beam in a straight trajectory with respect to the table plane; this is done by (slightly) tilting the mirrors along the trajectory.
In addition, the laser is positioned such that the polarization of the beam is vertical: this makes the wavefront shaping by the SLM more effective.

Then, objectives and scattering layer/diffuser must be at the right distance.
We want the first objective to be such that it, almost ideally, Fourier transforms the beam reflected from the SLM to the front surface of the scattering layer; we also set the apparatus so that the focus is created at $\sim$ 3mm behind the layer. To arrange this situation, we start by imaging the back-surface of the scatterer: this is done by moving the second objective and minimizing the blob of light that we see, which means that we are directly imaging the back-surface of the layer.
After, by hand because stages we had could not move of more than 2 mm, we move the second objective 3 mm towards the cameras.

We are still able to easily move the scattering layer in between the objectives thanks to the cage system: however, any move scrambles the alignment.

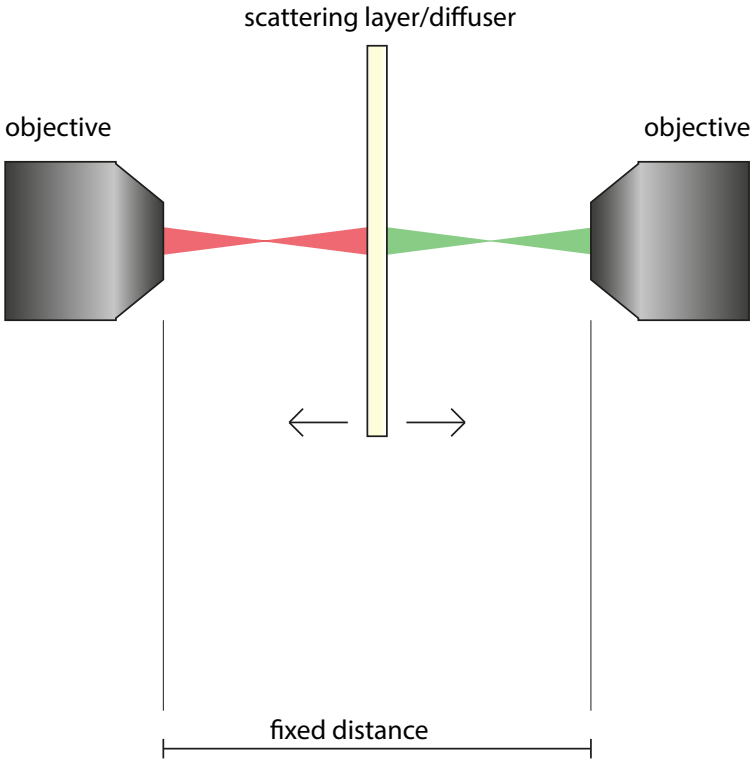


FIGURE 4.1: Scheme of the objectives and the scattering layer/diffuser: the fixed distance is shown.

The relative distance of the layer with respect to the two objectives is very important because it determines the speckle sizes. This is schematically shown in figure 4.1. This is due to two reasons: moving away the scattering layer from the first objective increases the width of the beam on the front surface of the layer and going closer to the second objective decreases the area we are looking at with the camera. We remind again that we optimize - create a focus - 3mm behind the scatterer.

In figure 4.2, one can see a speckle pattern before any process. It is B/W because each pixel returns a count: the higher the number the brighter the spot.

Beyond this basic optical preparation, we need to select the parameters for our software to perform well.
Always, the side of the optimization area is chosen as large as the speckle

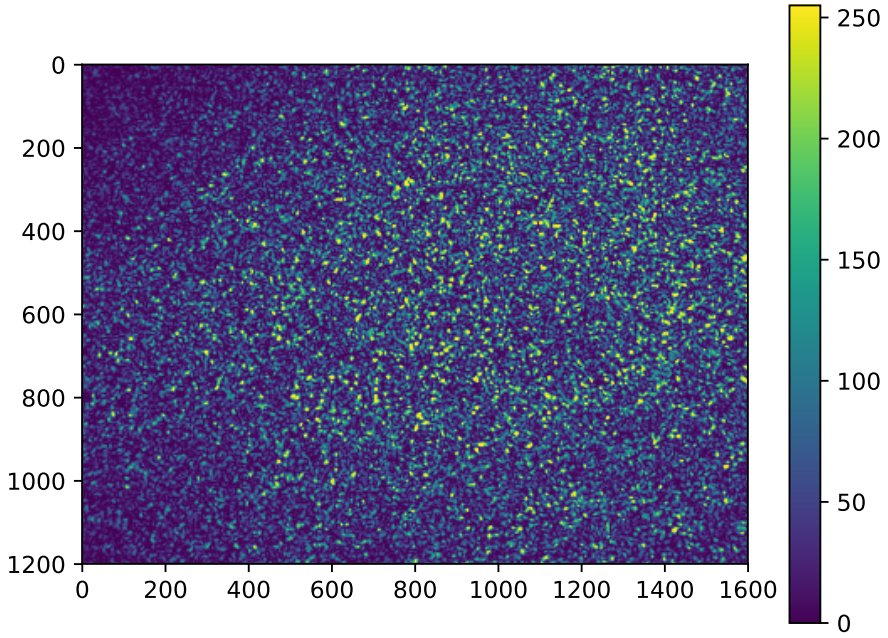


FIGURE 4.2: Speckle pattern is measured with a plastic scattering layer, a 532 Hz laser and the feedback camera. On the right side, the color map of the photo is shown.

size, the number of superpixels to be used is selected following the measurements which give us the best combination of superpixels to use for respectively random, pre-opimization and optimization pattern to reach a large enhancement.
The other main parameter is the exposure time.

### 4.1.1 Exposure time

The exposure time is the time that the camera is exposed to light; we wrote a script to choose it.

A picture is taken and two conditions, a lower and an upper boundary condition, are tested. The initial exposure time is manually inserted to be 'not far' from a suitable value: this is done by eye-looking at the picture on camera. Before the focus is created, the exposure time is increased if the pixels with value greater than a low threshold ($180 - 230$)) are less than 10% of the total number of pixels (lower boundary condition) while decreased if the saturated (255) pixels are more than 10% (upper boundary condition). These conditions are fine to achieve a visible enhancement already in the pre-optimization

process.
After the focus is created in the pre-optimization process, exposure time is changed if there are pixels with values out of the chosen range: minimum 185 and maximum 225. We do not want to see a full black or fully saturated picture.

## 4.2 Enhancement

The enhancement, $\eta$, is the figure of merit for the wavefront shaping. it represents how much brighter than initial average intensity the in-focus area is after optimization.

$$\eta = \frac{I_{focus}^{final}}{t_{final}} \frac{t_{initial}}{I_{100}^{initial}}, \tag{4.1}$$

Equation 4.1 is the formula that we use to measure the enhancement; $t_{final}$ and $t_{initial}$ represent respectively final and initial exposure time; $I_{focus}^{final}$ represents the intensity in the focus area after optimization while $I_{100}^{initial}$ represents the average intensity of an area 100 times the size of the focus area.

Taking into account the average intensity on a bigger area, instead of the in-focus intensity, is done to have consistent results: in figure 4.2, it is clear that the resulting in-focus intensity varies much if we focus on an initially bright (or dark) region.
On the other hand, after optimization, we want to know how bright the focus is and not the average intensity on a bigger area.

Changing exposure time during the measurement is something that I personally would not like to do: the reason behind is that stability and noises of the system can change and bring the system to a drastically different regime.
However it is needed: if we select a too short exposure time, we have more measurement noise; if we select a too long exposure time, images will be saturated and we cannot measure enhancement. We automatically choose exposure time in order to fulfill conditions described above.

To compare images with different exposure times, we divide the measured intensity with the exposure time.
If we have images a and b with intensity $I_a$ and $I_b$ and exposure times $t_a$ and $t_b$, with $t_a < t_b$, what we can compare is $\frac{I}{t}$, so that intensity is calculated per time unit.
That is the reason why the formula 4.1 includes initial and final exposure

time; these are the times set to take the pictures out of which we can calculate the intensity and thus the enhancement.

Expected enhancement range for the optimization lies between 800 and 1300, because of the number of superpixels used. Our best results are around the same values but, on average, the enhancement was between 100 and 300, a factor $\sim \frac{1}{4}$ difference.

To summarize, enhancement is calculated from measured intensity and exposure time of images taken before and after the optimization process. As explained above, the in-focus intensity is always related to the average intensity of an area 100 times bigger.
This is reliable in comparing measurements performed with very different parameters.

## 4.3 Wavefront Shaping

We use wavefront shaping to create a focus behind the thin scattering layer/diffuser.
There are many parameters, i.e. speckle size, the area of optimization, the exposure time but also the number of superpixels used at each step, that influence the achieved $\eta$.
In this section, we describe the way we perform wavefront shaping.

At the beginning of the project, we used two optimization steps, called pre-optimization and optimization, where we used the continuous sequential algorithm - that means updating the pattern on the SLM while performing the optimization process.
After noticing that setting the same number of superpixels - that means performing the same process twice - only allowed us to reach an enhancement in the second process, we decided to update the SLM with a random pattern at first.

### 4.3.1 Random pattern

An example of a random pattern is shown in figure 4.3.

The idea behind the random pattern is the following; if we start with a one-color-only SLM, we don't know when the voltage is inverted and which noise it generates although we know that a photo is taken only when the triggering signal is given: in this case, the noise propagates from the SLM to the beam and we cannot reach a regime when signal overcomes noise. It seems that

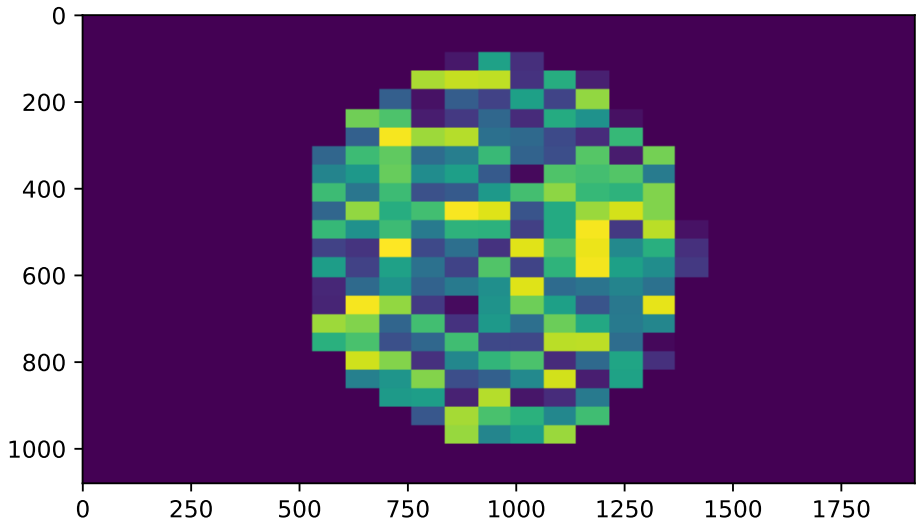


FIGURE 4.3: An example of random pattern.

there is some amplitude modulation, but our SLM should be phase modulation only.
Instead, if we use a randomly but uniformly distributed pattern, we know that reversing the voltage can generate noise but that noise is averaged by the randomness of the pattern.

The random pattern allowed us able to achieve a relative small enhancement in the pre-optimization step as well. If we could reach an enhancement in the magnitude order of $\approx 10$ for the pre-optimization, our final enhancement should be the best we can obtain ([26]).

### 4.3.2 Current method

When able to get a reasonable enhancement for the pre-optimization with the iterative algorithm, we decided to switch to the non-iterative algorithm. Main advantage is that there is no need to decrease the exposure time during the pre-optimization and optimization process: the exposure time is changed only before or after each of these processes. In fact, when testing different phases on each superpixel, the signal is too low to saturate the camera but large enough to optimize.

We perform wavefront shaping now with following steps:

- random pattern: a randomly uniformly distributed pattern is generated and screened on the SLM
- pre-optimization: to enhance the in-focus intensity, a pre-optimization pattern is generated and, finally, screened on the SLM
- optimization: to enhance the in-focus intensity, an optimization pattern is generated and, finally, screened on the SLM

Both pre-optimization and optimization are executed with the non-iterative algorithm: thus pre-optimization and optimization differs only by the number of superpixels.

## 4.4 Memory effect

After creating a focus, we want to be able to scan it around. This is achieved by exploiting the memory effect.
Being in Fourier configuration, on the front surface of the scattering layer means that we see the k-space of the beam reflected from the SLM, and consequently means that to impose a phase gradient to the beam (equivalent to tilting the beam on the surface), we have to shift the pattern on the SLM.
However, this is true if the front surface is precisely in the focus of the objective and if the SLM is imaged from infinity at the back focal plane of the same objective. Due to a possible alignment error, we might be slightly off.
In addition, we tried to tilt the pattern but I would need more time to analyze data. Recently, a combination of tilting and shifting has been used to create and scan a focus ([7]).

We expected to be able to scan the focus around a large area before the intensity is gone.

This area can be enlarged also by increasing the exposure time, although with two drawbacks.
The background intensity increases giving rise to a worse contrast, which we want large with this technique. Enhancement, as calculated in 4.1, decreases and so does the quality of our measurement: in fact, $\eta$ is a measure of our optimization ability and the larger $\eta$ the best we are doing.

As counterexample, we decided to focus on several different spots not by means of the memory effect but by directly optimizing on different points; this was done by changing the feedback area from the feedback camera.
Although, this brought us our best enhancement values, it is not viable as

technique: it usually requires long time before optimization is completed so it is not suitable for studying phenomena which have timescales shorter than hours.

## 4.5 Optimization time

The time needed for the optimization process depends on the number of superpixels used: for pre-optimization, we use between 300 and 500 active superpixels, while, for the optimization, we use between 1000 and 2000. This means that pre-optimization takes around 10 minutes and optimization around 30: this is not fast enough to be able to focus by optimization process in different spots.

The optimization time is linear with the number of superpixels and, on each superpixel, 6 different phases are tested: for an exposure time of 50000 $\mu$s, the process time for one superpixel is $0.05 \times 6$ s $+ 0.1$ s - this tenth of a second is added to be sure that the SLM updated to the new pattern - which corresponds to 0.4 seconds per superpixel; for an exposure time of 500000 $\mu$s, one superpixel needs 3.1 s to be processed.
Counting respectively around 350 superpixels for pre-optimization and 1900 for optimization, we need to wait 15 minutes for the short exposure time and almost 2 hours for the long one.

In addition, optimization times must be faster than the persistence time of the scattering layer/diffuser. The persistence time is the time at which the speckle pattern remains stable.

## 4.6 Virtual Object

We used a pinhole of 50 $\mu$m as virtual object to be imagined and scanned by the previously created focus.

# Chapter 5

# Results

In this chapter, results obtained are described in detail.

## 5.1 Wavefront shaping

In this section, results about the creation of the focus are shown.

In general, the optimization process is done using the non-iterative algorithm twice: first time we call it pre-optimization and second time optimization. Before the use of an initial random pattern, only pre-optimization and optimization were used.
If the same process was repeated twice during pre-optimization and optimization, with same number of SPs, we could only see an enhancement in the second step: unexpectedly, it seemed as the pre-optimization pattern was useful only to reach the right regime to be able, then, to get a real ($> 1$) enhancement. We found that a random pattern can help in achieving some enhancement during the pre-optimization: the goal was to achieve an enhancement of order 10 in the pre-optimization (which we did!).

### 5.1.1 Enhancement vs SP pre-optimization and random pattern

In figure 5.1, we see the enhancement obtained after pre-optimization versus the number of superpixels used.
The measurements were performed for different number of SPs in the random and in the pre-optimization pattern. Legend on figure 5.1 relates the color of each curve to the number of superpixels used in the random pattern. Each random pattern is generated with a uniformly random distribution of phases that we update on the SLM before starting the pre-optimization process.

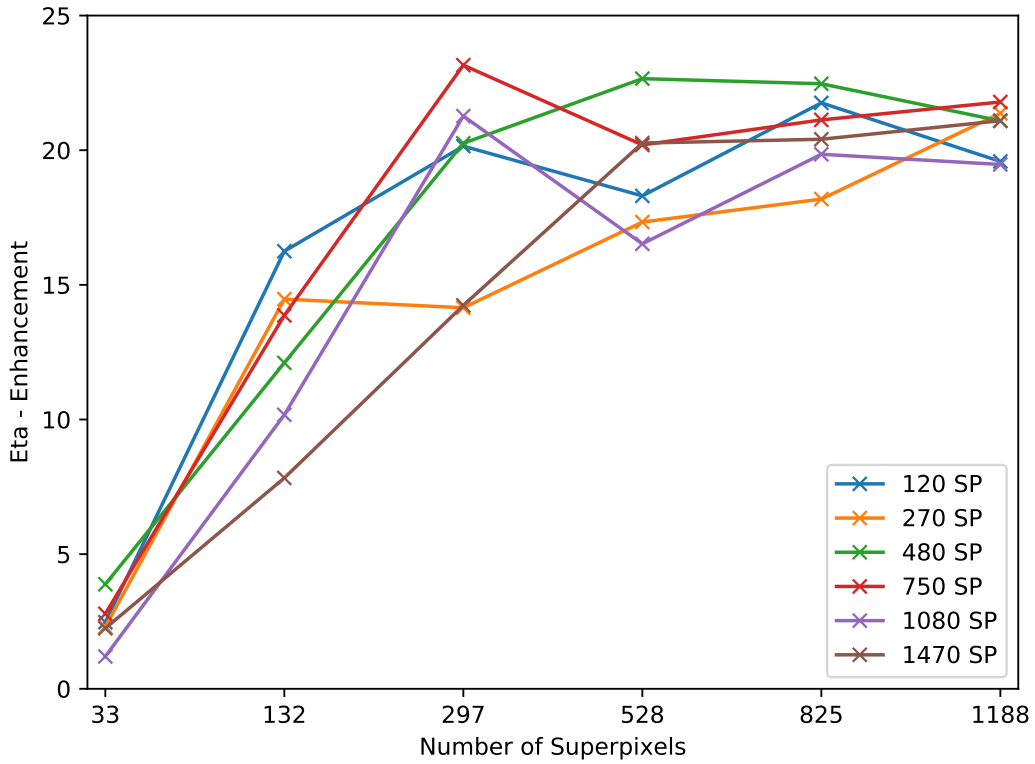


FIGURE 5.1: $\eta$ for pre-optimization is plotted with the number of superpixels used: the scale of the x-axis is not linear because we use to increase the number D of times that we divide each side of the SLM; that means that the number of used superpixels is proportional to $D^2$. This is measured for different random patterns: in the legend, the number of superpixels of the random pattern corresponding to each curve is shown.

As one can see, as the number of SPs increases, the enhancement increases. This is expected. In the end of the curves, sometimes we do not see an increase: it can be related to the duration of the measurement with a large number of SPs. In fact, if the persistence time is shorter than the duration, it is hard to achieve some enhancement.
We found that best combinations are $20 \times 20$ for random pattern and $30 \times 30$ for pre-optimization pattern or viceversa.

However, it is still unclear how the different number of SPs of the random pattern can influence the pre-optimization enhancement.
One explanation I can give myself is the following. Without random pattern the SNR (Signal to Noise Ratio) of one SP is 1 or more, so, as result, we cannot optimize. Apparently, a uniformly distributed random pattern brings to a regime where the SNR is less than 1 and we are thus able to achieve some enhancement.
Another option is that the SLM is not doing only phase modulation.
Another possible explanation is the following. When the wavefront is flat,

so when we do not update any random pattern, varying phase to one superpixel only introduces edges which could result in losses due to diffraction. Diffraction losses are balanced with improvements due to interference: in this case, we are not able to achieve any enhancement.

### 5.1.2 Enhancement vs SP optimization - different spots

In figure 5.2, enhancement obtained after optimization is shown versus the number of used superpixels: each line corresponds to a different focus position.
If the optimization process is fast enough we can always, instead of moving by means of the optical memory effect, optimize on a different spot: this could have as big advantage a large enhancement not influenced by any motion. However, this is not my case because each optimization process takes around 30 minutes/1 hour: respectively we need between 15 minutes, in the case of short exposure time of 0.4 s, and 1.9375 h for exposure time of 3.1 s.
On the grid, each step size is two times the speckle size, corresponding to 48 pixels on camera corresponding to 384 $\mu$m. The measurement was performed to ensure the ability to focus away from the center of the camera.

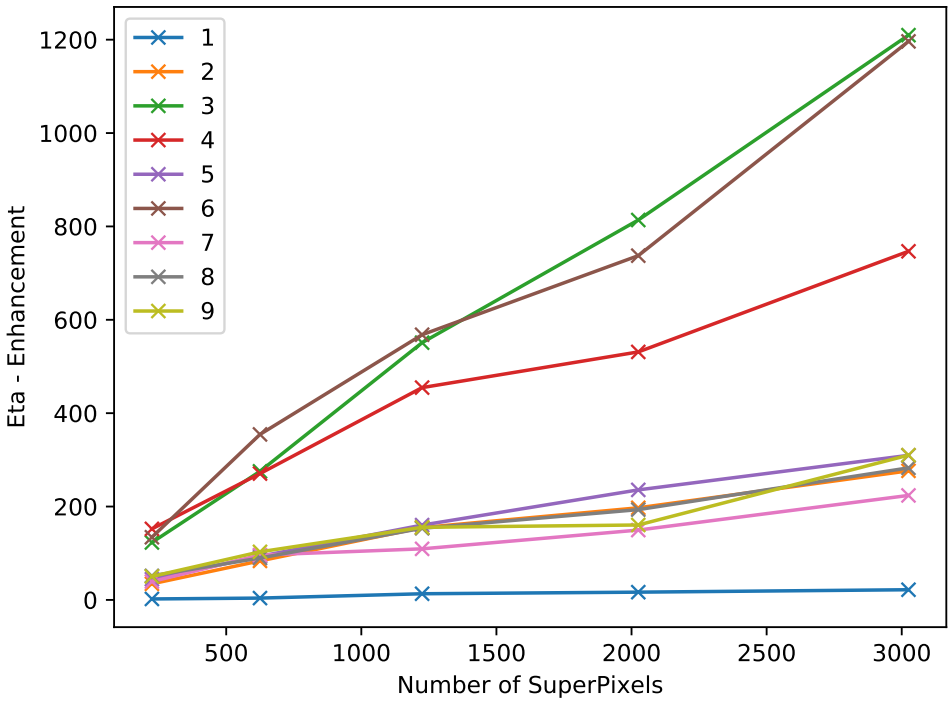


FIGURE 5.2: Enhancement after optimizing with different number of SPs in different focus positions, as shown if Figure 5.3.

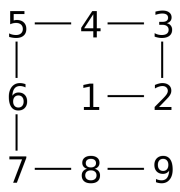


FIGURE 5.3: Numbers related to different focus positions: to point out that the ordering is not important.

We chose a number of SPs for the random pattern as $20 \times 20$ (the best results given by the measurements of subsection) with $30 \times 30$ for the pre-optimization pattern.

A possible explanation why the optimization on the central spot of the camera reaches such a low enhancement compared to the other positions is the following: the center of the camera is the portion usually used; if some pixels are damaged, they return a lower intensity so that the measured enhancement is much lower.

As expected, we find more enhancement when we use a larger number of SPs. But, there is no clear difference between optimization on different spots: it is unclear why different positions show different enhancement.
In addition, the variation of $\eta$ is wide: almost 3 magnitude orders.

To conclude, in figure 5.2, we show the best enhancement obtained: more than 1000. It is a nice result because it was reached in only some experiments, for example [4].
It is unclear why position 3 and 6 (and then 4) are the places where you can get the better enhancement: from theory it should not matter and $\eta$ should only increase linearly depending on the number of SPs used.

## 5.2 Image of focus, fit Gaussian and analysis method

Figure 5.4 shows an image of the intensity-enhanced focus with the contours given by the Gaussian fit used for analysis.

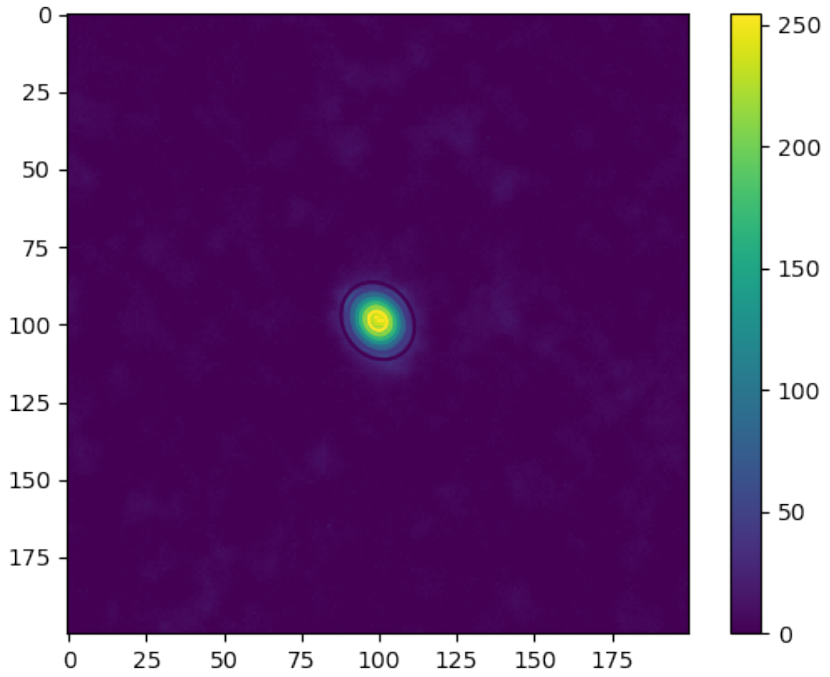


FIGURE 5.4: The figure shows the image of the focus on top of which is fit a 2D Gaussian function with contour lines. On the right side, the color map for the figure is shown.

To analyze the created focus, we cut off an image with size of $200 \times 200$ pixels: this is done so that the fitting process is much faster than working on full size images ($1600 \times 1200$).
A 2D Gaussian function is fit to the focus and used to retrieve the parameters.

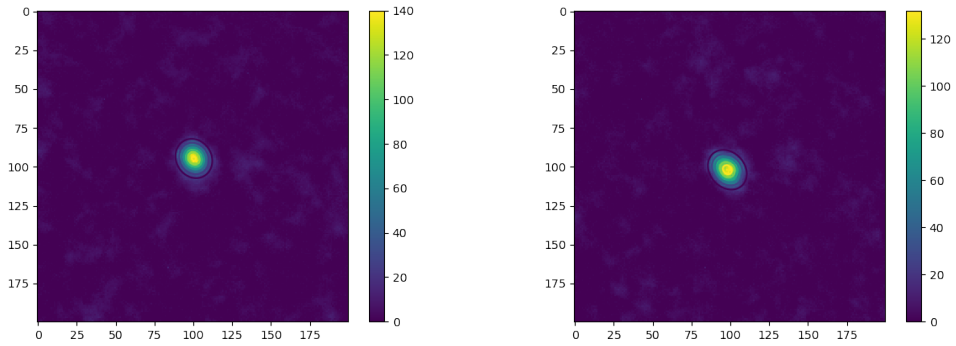


(A) Offset from camera center is (-5,-5). (B) Offset from camera center is (5,5).

FIGURE 5.5: Both figures represent the fit center for optimization pattern displaced of (a,b) pixels respectively in x and y direction.

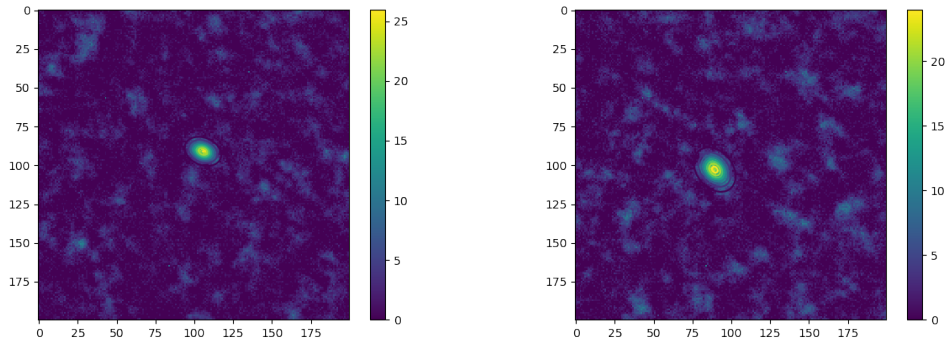

(A) Offset from camera center is (0,-15). (B) Offset from camera center is (0,15).

FIGURE 5.6: Both figures represent the fit center for focus displaced of (a,b) pixels respectively in x and y direction.

In figures 5.6 and 5.5, we show how the intensity decreases if we move the focus away from the position where we optimized on: the more we move away the more the intensity decreases. This can be seen in the fact that the intensities of the fit Gaussian functions show a decreasing trend : above 250 for the focus in the center as in figure 5.4, $160 - 170$ for centers moved of $\approx 7$ pixels as in figure 5.5, and finally $20 - 25$ for a motion of 15 pixels as in figure 5.6. We expect that the motion of the focus by means of the optical memory effect can lead to decrease in intensity of the same focus.
Last, I would like to point out that the more we move the focus, the more the average intensity of the background seems to increase: there is no real increase in the background but, as the in-focus intensity decreases, the ratio of background and in-focus intensity increases appearing as an increase in background average intensity.

## 5.3 In-focus intensity versus distance from the center

This section is about the intensity of the focus when moving the focus by means of optical memory effect.

In figure 5.7 and 5.8, we show the plot of in-focus intensity of fit 2D Gaussian versus shift of the focus from the position of optimization.
After moving the focus $40 \times 40 = 1600$ times, taking a picture each one and fitting with a 2D Gaussian, we show the plot of fit intensity versus distance of the foci from the center.
Some obviously non-real results are not in this plot: we discarded data that show foci in positions outside the cropped image ($200 \times 200$ pixels). So, if the fit focus is in position (a,b) with a,b $> 200$, it is not taken into account.

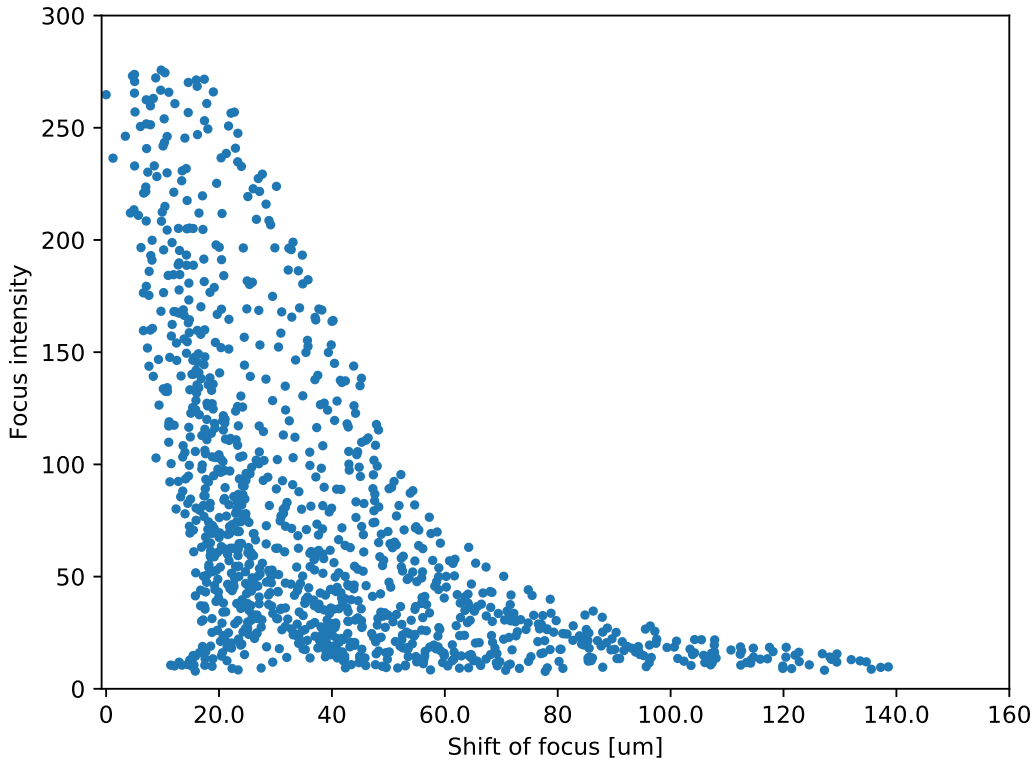


FIGURE 5.7: In-focus intensity of the fit Gaussian vs distance from the center of camera.

As one can see, the more we go away from where the focus is at first created, the more the intensity decreases. This is expected [5].
However, we would not expect such a broad variation from points that are at the same distance: initially we expect a line along which all the fit points should lie. In our case we do not see a line but an area: we see a broadening of what we expect.

Assuming that some pixels degrade the measurements implies that the real intensity corresponds to the best intensity achieved. If the previous assumption is used, this means taking into account only the outer points of figure 5.7 and 5.8. The curve drawn connecting outer data points is smooth which reasonably means that it represents the real curve.
Calculating the thickness of the scattering layer by inverting the optical memory effect and noticing that the full width at half maximum (FWHM) is $\approx 55$ $\mu$m, gives as result 30 $\mu$m: this value is reasonable. However, if 20 $\mu$m and 30 $\mu$m are respectively considered, the FWHM is expected to shift from $\approx 55$ $\mu$m to $\approx 80$ $\mu$m.

The difference between the two figures is that figure 5.7 was made before calibrating the SLM.
I am not sure whether calibration plays an important role at this point because shifting a pattern does not rely on having a calibrated SLM. However,

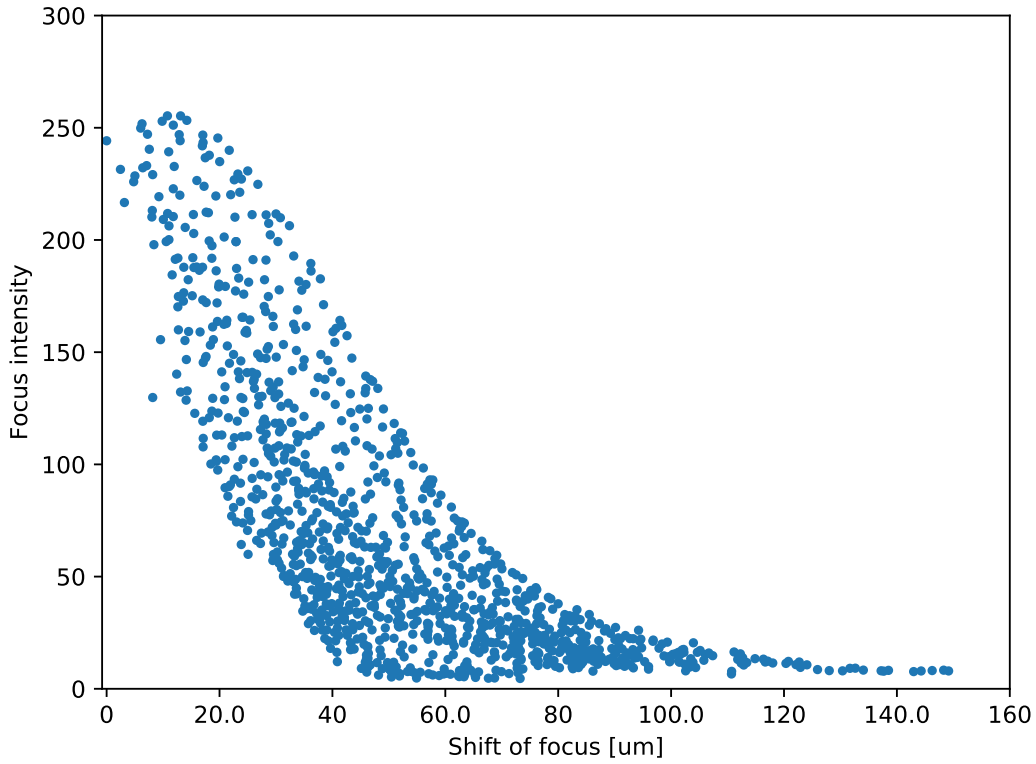


FIGURE 5.8: In-focus intensity of the fit Gaussian vs distance from the center of camera.

the non calibration can lead to misinterpretation: if we ignore that the SLM has a range broader than 2 periods, we could be testing the same phases i.e. 0 and $2\pi$,$\pi/2$ and $3\pi/2$.
What we can see is that with calibration the graph seems more narrow. However, the broadening is still there.

## 5.4 Plot of fit centers

In figures 5.9 and 5.10, the fit foci positions have been plotted on a 2D area which represents a cut of the $200 \times 200$ pixels picture. Again, fit centers which were out of the selected range are not taken into account: we assume that the fit happened on noise and not on a clear and sharp focus. For example, some foci apparently moved by 100 pixels with an uncertainty of more than the sizes of the picture: we do not use these data points.

The expectation is to see orthogonal straight lines, which we don't. However, figure 5.10, done after calibrating the SLM, seems already more tidy and ordered although the lines are still not orthogonal. In addition, most of them are curves and few are lines.
The expectation to see orthogonal and straight lines follows the fact that we

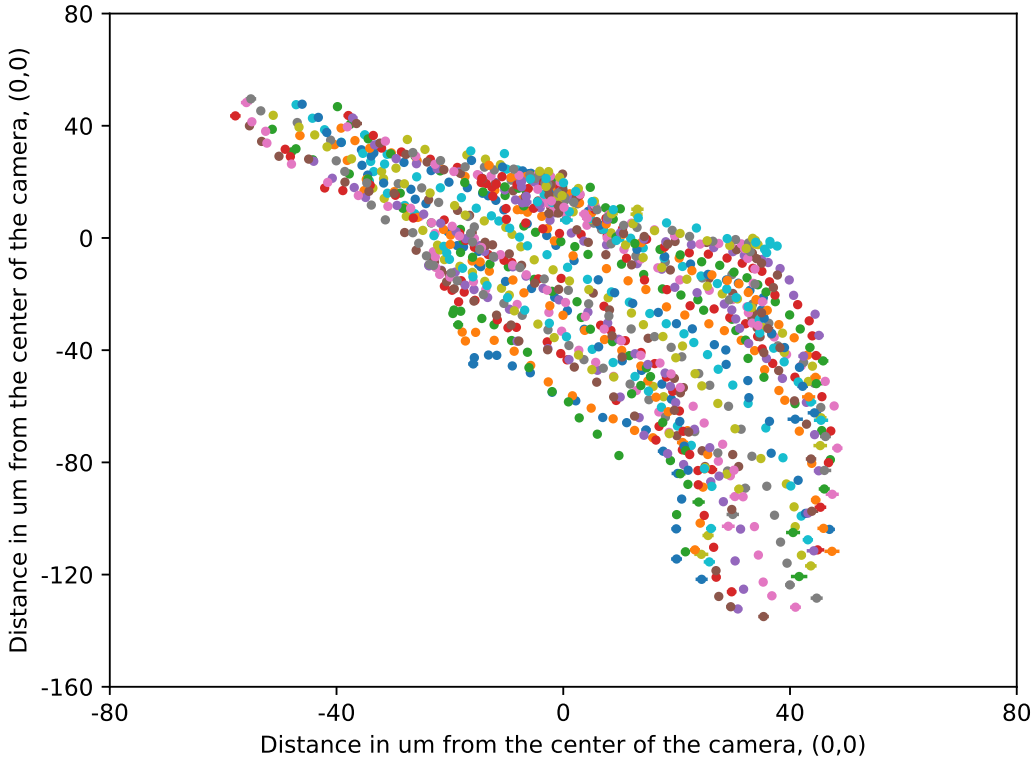


FIGURE 5.9: Centers of the fit Gaussian on a cut of the full figure before calibration.

are tilting the beam on the front-surface of the scattering layer along two orthogonal directions: each straight line should correspond to a full scan in one direction.
Again, the difference between figure 5.9 and 5.10 is that the former was taken with a non-calibrated SLM while the latter after calibration.

Having curves instead of lines can be due to the following reasons:

- the SLM could be curved (with second order distortion)
- there could be cylindrical distortions in my system
- Peter, who shared the optical table with me, was typing during many experiments: he introduced noise and mechanical instability

## 5.5 Conclusions

In-focus intensity is enhanced via wavefront shaping. However, enhancement is obtained only some times. A random pattern, updated before starting the pre-optimization process, makes the technique more robust: when

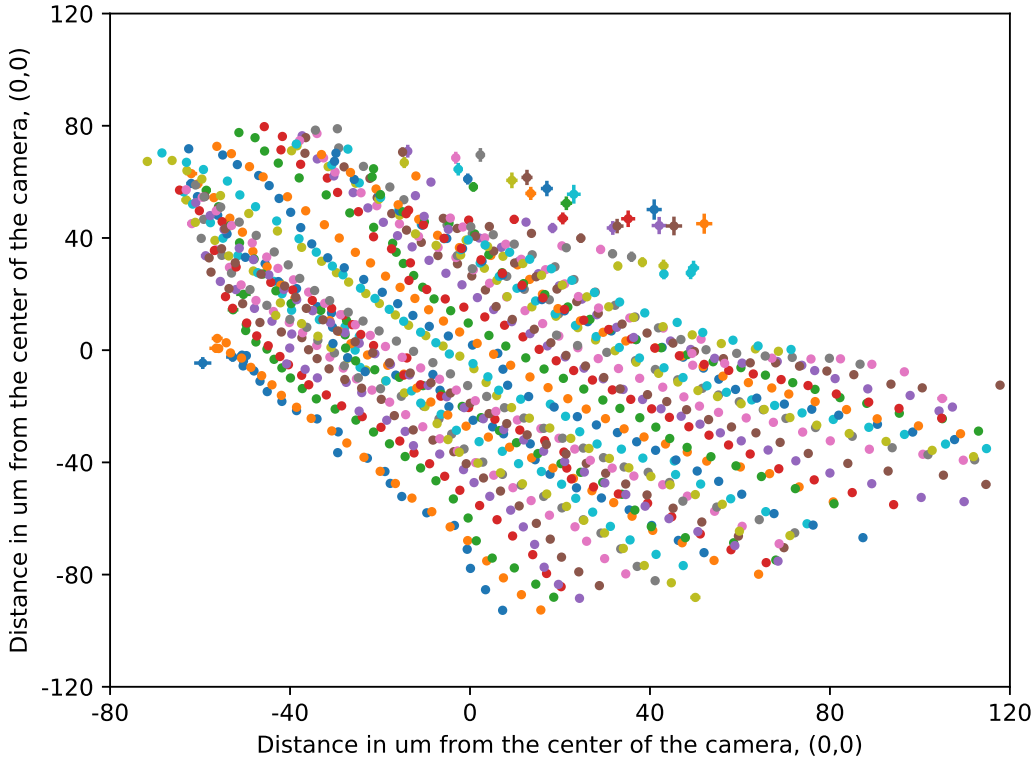


FIGURE 5.10: Centers of the fit Gaussian on a cut of the full figure after calibration.

using a random pattern, a real ( $> 1$ ) enhancement is achieved.

The created focus is moved by means of the memory effect. The motion works although it is still not ideal.
The angle of the memory effect is in the right range but the broadening of the curve is not: data points are expected to follow the profile of the curve in figure 5.7 and 5.8 but, instead, points are spread in a large region. The reason is still unknown.

# Chapter 6

# Conclusions and outlook

## 6.1 Conclusions

We were able to create an intensity-enhanced focus.
Achieved enhancement covers 3 magnitude orders: maximum enhancement obtained is over 1000. If the created focus is always, at least, 2 magnitude orders more than the background, we can use it to easily detect light scattered from the focus area and take images.
In addition, few experiments reported enhancement higher than 1000 and it can be considered a valuable result.

We wanted to scan the previously generated focus around: we were able to scan the focus in a reasonably large region: however, it is not clear why in-focus intensity does not depend only on the distance from the optimization spot.
We expected to be at the FWHM for $1.57^o$ but we found the FWHM at $1.04^o$: however, the error in the thickness of the scattering layer influences strongly this result.
As long as we shifted the pattern along the orthogonal axes of the SLM, we expected orthogonal lines and we obtained non-orthogonal curves.

We tested whether the light transmitted to the second camera increases when we create the focus: this light would interact with the object if the object was not a non-object (a pinhole, so that we only use the borders of our object).
This means that we can use wavefront shaping to select where interference is constructive: by choosing a spot for constructive interference, we select where the intensity-enhanced focus is. We usually want to choose the spot as the same of the object.

## 6.2 Outlook

As outlook, we would like to give ideas and doubts.

It is still unclear:

- such wide range of $\eta$
- a uniformly random pattern can initially help in achieving enhancement
- how to place the scattering layer perfectly orthogonal to the beam
- how to quickly retrieve the pattern to create focus

As future research, it could be interesting to implement the techniques described in chapter 2 so that it is possible to make comparisons between transmitted and reflected enhancement: is $\eta$ going to be the same or always different?

In addition, it is possible to check whether the *confocal* technique is better than the *total intensity* one; as well, one can compare the ratio between the techniques both in reflection and in transmission.

With both information on reflected and transmitted light, it could be possible to image an object from two sides: techniques that make use of both information can improve the contrast and the precision of taken images.

More on the theoretical side, discoveries in the field of scattering can bring insights on random matrix theory.

To conclude, humans must continue playing with light: a new perspective on an old question could be the discovery of this century!

# List of Figures

# Bibliography


[1] J. Bertolotti, E. G. van Putten, C. Blum, A. Lagendijk, W. L. Vos, and A. P. Mosk, "Non-invasive imaging through opaque scattering layers", *Nature*, vol. 491, 232–234, 2012. [Online]. Available: https://www.nature.com/articles/nature11578.

[2] A. P. Mosk, A. Lagendijk, G. Lerosey, and M. Fink, "Controlling waves in space and time for imaging and focusing in complex media", *Nat. Photonics*, vol. 6, 283–292, 2012. [Online]. Available: https://www.nature.com/articles/nphoton.2012.88.

[3] O. S. Ojambati, J. T. Hosmer-Quint, K.-J. Gorter, A. P. Mosk, and W. L. Vos, "Controlling the intensity of light in large areas at the interfaces of a scattering medium", *Phys. Rev. A*, vol. 94, p. 043 834, 4 2016. DOI: 10.1103/PhysRevA.94.043834. [Online]. Available: https://link.aps.org/doi/10.1103/PhysRevA.94.043834.

[4] E. van Putten, D. Akbulut, J. Bertolotti, W. Vos, A. Lagendijk, and A. Mosk, "Scattering lens resolves sub-100 nm structures with visible light", *Phys. Rev. Lett.*, vol. 106, 19 2011. [Online]. Available: https://link.aps.org/doi/10.1103/PhysRevLett.106.193905.

[5] I. Freund, "Looking through walls and around corners", *Physica A*, vol. 168, no. 1, pp. 49 –65, 1990, ISSN: 0378-4371. DOI: https://doi.org/10.1016/0378-4371(90)90357-X. [Online]. Available: http://www.sciencedirect.com/science/article/pii/037843719090357X.

[6] I. Freund, M. Rosenbluh, and S. Feng, "Memory effects in propagation of optical waves through disordered media", *Phys. Rev. Lett.*, vol. 61, pp. 2328 –2331, 20 1988. [Online]. Available: https://link.aps.org/doi/10.1103/PhysRevLett.61.2328.

[7] G. Osnabrugge, R. Horstmeyer, I. N. Papadopoulos, B. Judkewitz, and I. M. Vellekoop, "Generalized optical memory effect", *Optica*, vol. 4, no. 8, pp. 886–892, 2017. DOI: 10.1364/OPTICA.4.000886. [Online]. Available: http://www.osapublishing.org/optica/abstract.cfm?URI=optica-4-8-886.

[8] J. Goodman, *Introduction to fourier optics*. May 2017.

[9] C. Cave project. (). Single vs multi scattering, [Online]. Available: http://www.cs.columbia.edu/CAVE/projects/ptping_media/.

[10] E. van Putten, "Disorder-enhanced imaging with spatially controlled light", PhD thesis, University of Twente, 2011.

[11] I. M. Vellekoop and C. M. Aegerter, "Scattered light fluorescence microscopy: Imaging through turbid layers", *Opt. Lett.*, vol. 35, no. 8, pp. 1245–1247, 2010. DOI: 10.1364/OL.35.001245. [Online]. Available: http://ol.osa.org/abstract.cfm?URI=ol-35-8-1245.

[12] M. Kim, W. Choi, Y. Choi, C. Yoon, and W. Choi, "Transmission matrix of a scattering medium and its applications in biophotonics.", *Opt. Express.*, vol. 23, no. 10, pp. 12 648–12 668, 2015. DOI: 10.1364/OE.23.012648. [Online]. Available: http://www.opticsexpress.org/abstract.cfm?URI=oe-23-10-12648.

[13] I. M. Vellekoop and A. P. Mosk, "Universal optimal transmission of light through disordered materials", *Phys. Rev. Lett.*, vol. 101, p. 120 601, 2008.

[14] S. F. Liew, S. M. Popoff, A. P. Mosk, W. L. Vos, and H. Cao, "Transmission channels for light in absorbing random media: From diffusive to ballistic-like transport", *Phys. Rev. B*, vol. 89, p. 224 202, 22 2014. [Online]. Available: https://link.aps.org/doi/10.1103/PhysRevB.89.224202.

[15] I. M. Vellekoop, "Feedback-based wavefront shaping", *Opt. Express*, vol. 23, no. 9, pp. 12 189–12 206, 2015. [Online]. Available: http://www.opticsexpress.org/abstract.cfm?URI=oe-23-9-12189.

[16] I. M. Vellekoop, "Controlling the propagation of light in disordered scattering media", PhD thesis, University of Twente, 2008. [Online]. Available: https://arxiv.org/abs/0807.1087.

[17] J. G. Fujimoto, C. Pitris, S. A. Boppart, and M. E. Brezinski, "Optical coherence tomography: An emerging technology for biomedical imaging and optical biopsy", *Neoplasia*, vol. 2, no. 1, pp. 9 –25, 2000, ISSN: 1476-5586. DOI: https://doi.org/10.1038/sj.neo.7900071. [Online]. Available: http://www.sciencedirect.com/science/article/pii/S1476558600800172.

[18] F. Helmchen and W. Denk, "Deep tissue two-photon microscopy", *Nat. Methods*, vol. 2, pp. 932–40, 2006. [Online]. Available: https://www.researchgate.net/publication/7470101_Deep_tissue_two-photon_microscopy.

[19] I. M. Vellekoop and A. P. Mosk, "Focusing coherent light through opaque strongly scattering media", *Opt. Lett.*, vol. 32, no. 16, pp. 2309–2311, 2007. DOI: 10.1364/OL.32.002309. [Online]. Available: http://ol.osa.org/abstract.cfm?URI=ol-32-16-2309.

[20] T. Chaigne, O. Katz, A. C. Boccara, M. Fink, E. Bossy, and S. Gigan, "Controlling light in scattering media non-invasively using the photoacoustic transmission matrix", *Nat. Photonics*, vol. 8, 58–64, 2014. [Online]. Available: https://www.nature.com/articles/nphoton.2013.307.

[21] S. M. Popoff, G. Lerosey, R. Carminati, M. Fink, A. C. Boccara, and S. Gigan, "Measuring the transmission matrix in optics: An approach to the study and control of light propagation in disordered media", *Phys. Rev. Lett.*, vol. 104, p. 100 601, 10 2010. DOI: 10.1103/PhysRevLett.104.100601. [Online]. Available: https://link.aps.org/doi/10.1103/PhysRevLett.104.100601.

[22] C. OBIS. (). Coherent obis, [Online]. Available: https://www.coherent.com/lasers/main/obis-lasers.

[23] Holoeye. (). Holoeye pluto 1, [Online]. Available: https://holoeye.com/spatial-light-modulators/.

[24] wavefrontshaping.net. (). Slmpy, [Online]. Available: https://github.com/wavefronthsaping/slmPy.

[25] Mabl. (). Pypylon, [Online]. Available: https://github.com/dihm/PyPylon.

[26] H. Yilmaz, "Advanced optical imaging with scattering lenses", English, PhD thesis, University of Twente, 2015.